Wnt and the Cancer Niche: Paracrine Interactions with Gastrointestinal Cancer Cells Undergoing Asymmetric Cell Division

Hong-Wu Xin[1], Chenwi M. Ambe[1], Satyajit Ray[1], Bo-Kyu Kim[1], Tomotake Koizumi[1], Gordon W. Wiegand[1], Danielle Hari[1], John E. Mullinax[1], Kshama R. Jaiswal[1], Susan H Garfield[2], Alexander Stojadinovic[3,4], Udo Rudloff[1], Snorri S Thorgeirsson[2,*], Itzhak Avital[1,4,5*]

[1]Surgery Branch, [2]Laboratory for Experimental Carcinogenesis, Center for Cancer Research, National Cancer Institute, National Institutes of Health, Bethesda, MD 20892, USA; [3]Department of Surgery, Division of Surgical Oncology, Walter Reed National Military Medical Center, [4]Department of Surgery, Uniformed Services University of the Health Sciences, Bethesda, MD; [5]Bon Secours Cancer Institute, Richmond, VA 23230, USA.

Running Title: Asymmetric Cell Division in GI Cancers

Correspondence:

*** Snorri S. Thorgeirsson, M.D., Ph.D.**
Head, Center of Excellence in Integrative Cancer Biology and Genomics
Chief, Laboratory of Experimental Carcinogenesis
Center for Cancer Research
National Cancer Institute, NIH
37 Convent Drive MSC 4262,
Building 37, Room 4146A,
Bethesda, MD 20892-4262, USA
Phone: 1+(301) 496-1450(O)
Phone: 1+(301) 496-1935(W)
Fax: 1+ (301) 496-0734
E-mail: snorri_thorgeirsson@nih.gov

Or

*** Itzhak Avital, MD**
Executive Medical Director
Bon Secours Cancer Institute
Richmond, VA 23230, USA.
Email: itzhak.avital@gmail.com

Key words: Cancer-Stem-Cells, Asymmetric-Cell-Division, Non-Random-Chromosomal-Cosegregation, and Microenvironment**.**

Word count - excluding title page, abstract, summary, acknowledgement, author contribution, interest conflict, references, figures and tables: **3107**.

List of abbreviations:

ACD-NRCC: Asymmetric Cell Division with non-Random Chromosomal Cosegregation
SCD: Symmetric Cell Division
ACD: Asymmetric Cell Division
MACS: Magnetic Activated Cell Sorting
SP: Side population
NSP: Non-Side Population

ABSTRACT

Objective: Stem-like cancer cells contribute to cancer initiation and maintenance. Stem cells can self-renew by asymmetric cell division (ACD). ACD with non-random chromosomal cosegregation (ACD-NRCC) is one possible self-renewal mechanism. There is a paucity of evidence supporting ACD-NRCC in human cancer. Our aim was to investigate ACD-NRCC and its potential interactions with the cancer niche (microenvironment) in gastrointestinal cancers.

Design: We used DNA double and single labeling approaches with FACS to isolate live cells undergoing ACD-NRCC.

Results: Gastrointestinal cancers contain rare subpopulations of cells capable of ACD-NRCC. ACD-NRCC was detected preferentially in subpopulations of cells previously suggested to be stem-like/tumor-initiating cancer cells. ACD-NRCC was independent of cell-to-cell contact, and was regulated by the cancer niche in a heat-sensitive paracrine fashion. Wnt pathway genes and proteins are differentially expressed in cells undergoing ACD-NRCC vs. symmetric cell division. Blocking the Wnt pathway with IWP2 (WNT antagonist) or siRNA-TCF4 resulted in suppression of ACD-NRCC. However, using a Wnt-agonist did not increase the relative proportion of cells undergoing ACD-NRCC.

Conclusion: Gastrointestinal cancers contain subpopulations of cells capable of ACD-NRCC. Here we show for the first time that ACD-NRCC can be regulated by the Wnt pathway, and by the cancer niche in a paracrine fashion. However, whether ACD-NRCC is exclusively associated with stem-like cancer cells remains to be determined. Further study of these findings might generate novel insights into stem cell and cancer biology.

Targeting the mechanism of ACD-NRCC might engender novel approaches for cancer therapy.

INTRODUCTION

Stem cells can self-renew by symmetric cell division (SCD) or asymmetric cell division (ACD) where each daughter cell might assume different fates. Asymmetric cell division with non-random chromosomal cosegregation (ACD-NRCC) is a putative mechanism of cell self-renewal. However, ACD-NRCC is not necessarily indicative of self-renewal or asymmetric fate of daughter cells.

ACD-NRCC is defined as that each chromosome in a stem cell contains one template DNA strand that is conserved during ACD (figure 1A) [1]. By maintaining the template DNA strands within one daughter cell, stem cells can avoid accumulation of mutations stemming from DNA replication errors. Although, this principle has been demonstrated in various cells [2] some investigators were unable to confirm the existence of ACD-NRCC [3-8]. These inconsistent findings within the same cell types have provoked controversy, and have suggested a contributory role of the cancer niche/microenvironment [1-5, 7-12]. It's known that niche plays an important role in regulating stem cell ACD via Wnt signaling [13], however a role of niche via Wnt signaling has not been reported in regulating ACD-NRCC. Recently, we have demonstrated ACD-NRCC in real time, in live cells using real time confocal cinematography [14].

Gastrointestinal cancers may develop in tissues harboring cells that undergo ACD-NRCC [1, 15, 16]. Previously, detection of ACD-NRCC relied exclusively on fixed cells, which hindered correlative gene expression and functional studies [2, 9]. Instead, we chose to isolate live cells undergoing ACD-NRCC and study this unique cell division process in gastrointestinal cancer cells, and investigate their potential interactions with the cancer niche. Elucidating the mechanisms of ACD-NRCC (and potential self-renewal) in cancer cells may provide novel

insights into cancer maintenance and establish the basis for novel therapeutic approaches, which may target ACD-NRCC.

MATERIALS AND METHODS

Cells

Cells and culture conditions used in this study are detailed in table S1.

DNA double-labeling-procedure

DNA double-labeling technique was used to detect ACD-NRCC (figure 1B, Materials and Methods, table S1, S2 and S3) [9, 17, 18]. DNA double labeling was performed with minor modifications, as previously described by Rando et al. (figure 1B, figure S1A, and Supplementary methods) [9]. To observe cells arrested during mitosis, cells were plated singly with and without 2μM Cytochalasin D (Sigma, figure S1B and table S3). Double labeling was done with and without Wnt antagonist (10 μM of IWP2, Stemgent). siRNA-TCF4 (ON-TARGETplus, Dharmacon) or control siRNA (Dharmacon) were transfected using Lipofectamine-2000 according to manufacturer instruction (Invitrogen, Supplementary methods).

Immunofluorescence staining

Immunofluorescence staining was performed as previously described by Rando TA et al. with minor modifications (Supplementary methods) [9].

Fluorescence confocal microscopy

In order to accurately detect cells arrested in cytokinesis, we scored only isolated couplets, 100-130 couplets per condition, in triplicates (n=3 to 15). Confocal images and Z-stacks were generated with Bitplane's (Zurich, Switzerland) and Imaris software (v6.0). To clearly define the positions of the nuclei, 3D rendering images were obtained (figure 2, Supplementary figure S2, Supplementary methods). TCF4 staining-intensity was measured using LSM ImageBrowser 4.0 (Zeiss).

Isolation of live cells undergoing ACD-NRCC and live label retaining cancer cells (LRCC)

Live cells undergoing ACD-NRCC and live LRCC were isolated as previously described in Hari et al., and Xin et al. (Supplementary figure S3A) [14, 19].

Cell viability and toxicity assays

Cell viability was measured using kit-8 (Dojindo, Japan) and cell toxicity using the ApoTox-Glo assay kit (Promega, Madison, WI) according to the manufacturer protocol (Supplementary Methods).

Isolation and analysis of the side population

Side population (SP) cells were isolated as previously described (Supplementary methods, figure 3A-B) [20]. SP cancer cells are thought to represent putative tumor-initiating/cancer-stem-cells (figure 3A-B, table S8) [21]. SP and non-SP cells of liver cancer cells were plated initially at very low concentration and allowed to proliferate.

CD133+ cell isolation

CD133+ and CD133- cells were isolated and enriched over a second column by magnetic-activated cell sorting *(*MACS*),* using the indirect CD133 MicroBead kit (Miltenyi Biotec Inc., Auburn, CA, USA) according to manufacturer's protocol (Supplementary methods).

Conditioned media

Conditioned media were collected aseptically, filtered through 0.22 µm filter units, and mixed with normal growth media at a ratio of 1:3 (figure 4A, supplementary methods). Denatured conditioned media from CD133-/CD133+ dual chambers was boiled for 5 minutes, and 5% FBS was added to a total protein concentration equal to normal growth media. Specific gravity, pH and protein concentration were determined with Specific Gravity Bottle (Crystalgen, Inc., USA), pH Meter (HANANA instruments, USA), and Spectrophotometer (Thermo Fisher Scientific, USA).

Gene expression analysis

Total RNA was isolated using miRNeasy Mini kit and RNase-Free DNase Set (QIAGEN) following the manufacturer's protocol. All reagents for genomic DNA elimination, reverse-transcription, pre-amplification, and real-time qRT-PCR experiments for Human Stem Cell Pathway, Wnt and Pluripotency Pathway Arrays were done following the manufacturer's protocol (SABiosciences, Frederick, MD). Primers for individual genes: TCF4, TCF7, SOX17 and CSNK2A1 were purchased from Qiagen. We used the Ingenuity Pathway software for pathway analysis (IPA 9.0, supplementary methods)

Statistics

For full discussion see supplementary statistics. In brief, for detecting any ACD-NRCC, we used the exact binomial test with a null hypothesis of 0.00001. (B) To test for significance of the relative proportions of cells undergoing ACD-NRCC between tested groups, we used the Poisson method (figure 3C). (C) For the observed effect of the niche on ACD via non-random chromosomal cosegregation (figure 4A), we used the Fisher's exact test. Statistical significance was defined as p value <0.05.

RESULTS

Subpopulations of gastrointestinal cancer cells undergo ACD-NRCC.

Symmetrically dividing cells incorporated both nucleotides (IdU and CldU) into the nuclei of both daughter cells. Cells undergoing potential ACD-NRCC incorporated both nucleotides into only one of the daughter cells' nuclei while the other nucleus incorporated only one nucleotide (figure 2A-B, movie S1 and figure S2). Reverse labeling resulted in a similar pattern (figure 2B-v, figure S2B and table S4). We validated these results in 7 different cell lines and fresh surgical specimens using this DNA double labeling method; ACD-NRCC was observed in 1.5% to 6.3% (n=21) of cells tested (table S5). To identify asymmetrically dividing cells, we used confocal microscopy, and confirmatory Z-stacking with three-dimensional-rendering of cells arrested in cytokinesis-mitosis (figure 1B, 2, and S2). We further validated ACD-NRCC by isolating live cells undergoing ACD-NRCC using flow-cytometry (1.6% ± 0.3%, n=17; figure S3B-C, Materials and Methods). Cell viability and toxicity were tested with and without labeled-nucleotides. No statistically significant differences were evident between cells undergoing ACD-NRCC vs. SCD (figure S3D-E).

ACD-NRCC is a statistically significant phenomenon, occurring in 1 to 6% of 14 cancer cell lines ($p<0.0001$, n=63, supplementary-statistics), and in non-malignant liver cells (THLE-2 and THLE-3: 1.3% ± 0.3%, and 2.6 ± 0.6%, respectively) as demonstrated in three different methods (table S5-to-S7). In addition to the methods above, these results were validated using two additional FACS-based-methods: (1) double labeling FACS-based method to isolate 25,630 of 1,026,314 cells undergoing ACD-NRCC (figure S3, table S6); (2) single labeling FACS-based method to isolate live cells undergoing ACD-NRCC (table S7, Materials and Methods). The single labeling method yielded over 5 million cells undergoing ACD-NRCC derived from 11 different cell lines and cells from fresh surgical specimens.

Side-Population (SP) cancer cells undergo ACD-NRCC.

At one week, SP cells generated non-SP cells while non-SP cells generated only more non-SP cells (figure 3C, supplementary statistics) [20]. At one, two and five weeks SP cells exhibited 0%, 1%, and 3.2% ACD-NRCC, respectively ($p<0.0034$, n=3). Non-SP cells did not undergo ACD-NRCC, during the same time periods (P=0.024). To validate these findings, we isolated SP and non-SP cells from four different gastrointestinal cancers and melanoma. SP and non-SP cells were cultured for three weeks and tested for ACD-NRCC. In a blinded experiment, we detected ACD-NRCC only in SP cells (1.8% ± 0.33, p=0.004, n=12). OV6 is a marker associated with liver progenitors; it was found to segregate with the template DNA strand in SP cells undergoing ACD-NRCC; it was not detected in non-SP cells (figure S4) [22].

The cancer niche interacts with CD133+ cells undergoing ACD in a paracrine fashion.

CD133+ cells are thought to represent another class of putative tumor-initiating/cancer-stem-cells [23]. We detected ACD-NRCC in whole liver cancer cell-lines (1.0% ± 0.05, n=3). The absence of ACD-NRCC in either CD133+ or CD133-negative cells alone, prompted us to test for potential interactions between CD133+ and CD133-negative cells, using a dual chamber culturing system with semi-permeable membrane. We detected ACD-NRCC when CD133+ cells were in direct contact with CD133-negative cells (1.3% ± 1.0, n=3). Using the dual-chamber culture system, ACD-NRCC was detected in CD133+ cells (2.0% ± 1.0, n=6) that were exposed indirectly to CD133-negtive cells (figure 4A). Conversely, no ACD-NRCC was detected in CD133-negative cells indirectly exposed to CD133+ cells (Supplementary Materials and Methods). These results support our previous data investigating SP and non-SP cells, suggesting that ACD-NRCC is preferentially detected in SP and CD133+ cells.

Consequently we hypothesized that the cancer niche, i.e. the non-stem-cancer-cell population (CD133-negative cells), interacts indirectly with CD133+ cells undergoing ACD-NRCC. Therefore, we tested the effect of various conditioned media on ACD-NRCC (figure 4A). These experiments were conducted with the scientist testing for ACD-NRCC blinded to the conditions being tested (n=6). The physical properties of the conditioned media and the fresh media (pH, protein concentration and specific gravity) were not significantly different (P>0.05). Conditioned media from dual-chambers (containing CD133+ and CD133-negative cells), and from CD133-negative cells alone induced CD133+ cells to undergo ACD-NRCC (2.6% ± 0.8, and 3.1% ± 0.3, respectively). ACD-NRCC was not detected in CD133+ cells cultured in conditioned media from CD133+ cells (p=0.0001) or in CD133+ cells cultured alone (p=0.014), in contrast to conditioned media from dual-chambers. CD133-negative cells (cancer niche cells) did not undergo ACD-NRCC (p=0.014).

These results were further validated in blinded experiments aimed at determining whether heat-denaturation of the conditioned media would abrogate ACD-NRCC (figure 4B). ACD-NRCC was neither detected in CD133+ cells grown in heat-denatured conditioned media from dual chambers ($p=0.023$), nor in CD133+ cells alone (negative control). ACD-NRCC was detected in CD133+ cells cultured in media from dual chambers without heat-denaturation ($p=0.028$, positive control).

Taken together our data suggest that ACD-NRCC is preferentially detected in SP and CD133+ cells, and that the cancer niche/microenvironment can interact with cells undergoing ACD-NRCC in a heat-sensitive paracrine fashion.

The WNT pathway's transcription factor TCF is asymmetrically localized in cells undergoing ACD.

The Wnt pathway plays an important role in stem cells biology, self-renewal, and stem cells pluripotency [24, 25]. Using similar method for the detection of ACD-NRCC (Materials and Methods), we tested 6 key Wnt proteins from each of the 3 cellular compartments (cell membrane, cytoplasm and nucleus) in liver cancer cells undergoing mitosis. Only TCF4 was distributed asymmetrically (3.1% ± 1.5; 19/619 mitoses, n=3), while Frizzled7, LRP5, Axin2, APC and β-catenin were distributed symmetrically in all cells tested (figure 5A-B, Materials and Methods). To further validate these results, we tested TCF4 gene expression in isolated cells undergoing ACD-NRCC, and cells undergoing SCD (figure S3). Using real-time qRT-PCR,

TCF4 was up regulated in cells undergoing ACD-NRCC when compared to cells undergoing SCD in all cell lines tested (3.8 ± 0.4 fold, $p< 0.00003$, figure 5C).

To further test potential interactions between the Wnt pathway and ACD-NRCC, we performed comprehensive Wnt gene expression analysis on liver cancer cells undergoing SCD vs. ACD-NRCC (Materials and Methods). Of 84 tested Wnt genes, only 5 were differentially expressed in cells undergoing ACD-NRCC: CSNK2A1, which activates the Wnt pathway (61.7 ± 9.1 fold, $p=0.024$), TCF4 (3.8 ± 0.4 fold, $p< 0.00003$), TCF7 (13.1 ± 6.5 fold, $p=0.038$), Sox17 (7.4 ± 1.3 fold, $p=0.0082$), and RB1 (-3.86 ± 0.28 fold, $p<0.011$; figure 5D). These data were validated using qRT-PCR for individual genes (figure S5). Using the ingenuity pathway analysis tool, and stem cells gene expression analysis (figure S6), we propose a pathway map for cells undergoing ACD-NRCC (figure S7).

Inhibition of Wnt suppresses ACD-NRCC and the asymmetric expression of Wnt genes

We found that several Wnt pathway genes are differentially expressed in cells undergoing ACD-NRCC vs. SCD. Therefore, we tested the effects of Wnt activation and inhibition on ACD-NRCC (Materials and Methods). The rate of ACD-NRCC was unaffected by Wnt activation with Wnt3 (Wnt agonist). We used the Wnt3 agonist because we found that Wnt3-receptor is expressed equally on cells undergoing ACD-NRCC or SCD. Because we did not detect changes in the rate of ACD-NRCC after activation of the Wnt pathway via Wnt3 receptor, we next tested the effects of Wnt inhibition on ACD-NRCC. The effects of IWP2 (Wnt-antagonist) and siRNA-TCF4 on ACD-NRCC were then tested. Without affecting cell proliferation (figure 6A) a

5-to-12 fold reduction in the rate of ACD-NRCC was evident in live cells after treatment with IWP2 (5.1% ± 0.3% vs. 1.1% ± 0.1%, p=0.0087 for PLC/PRF/5; and, 2.5% ± 0.5% vs. 0.2% ± 0.1%, p=0.0069 for HuH-7; figure 6B). The ability to detect ACD-NRCC and asymmetric distribution of TCF4 protein in fixed cells was abolished by siRNA-TCF4 (2.1% ± 0.1% vs. 0, p=0.0033; figure 6C-D). IWP2 reversed or reduced the expression pattern of TCF4 (-17.2 ± 6.1 fold, p=0.0096), TCF7 (-14.5 ± 4.0 fold, p=0.014), Sox17 (0.4% ± 0.9 fold, p=0.85) and CSNK2A1 (0.7 ± 1.1% fold, p=0.59; figure 5, 6E and S5). IWP2 and siRNA-TCF4 reduced the expression of TCF4 protein by 63% (15.6 ± 2.0 vs. 5.7 ± 0.9, p=0.011) and 61% (15.6 ± 2.0 vs. 6.1 ± 0.2, p=0.0093; figure 6F, figure S8). These results implicate the Wnt pathway in ACD-NRCC.

DISCUSSION

Albeit controversial, recent evidence suggests the existence of stem-like tumor initiating cancer cells. ACD-NRCC is one potential way by which stem cells self-renew. Here we show that ACD-NRCC was detected preferentially in SP and CD133+ cells. ACD-NRCC occurred independent of cell-to-cell contact; instead, the microenvironment seemingly induced CD133+ cells to undergo ACD-NRCC in a heat-sensitive paracrine fashion. Mechanistically, we show that cells undergoing ACD-NRCC segregate asymmetrically the Wnt transcription factor TCF, and other Wnt genes. ACD-NRCC was unaffected by agonist-dependent Wnt pathway activation; however, inhibition of Wnt and knock down of TCF resulted in a significant suppression of ACD-NRCC.

Pine et al reported detection of ACD-NRCC in fixed lung cancer cells [11]. Here we show ACD-NRCC in several fixed and extend the findings to live gastrointestinal cancer cells. We validated these observations using two methods: DNA double and single labeling (label retention) [9, 17, 18]. The rate of ACD-NRCC detection was comparable between the two methods. Once thought to be a rare phenomenon, it is possible that ACD-NRCC occurs more commonly, and amongst cancers of diverse origins.

Observing this phenomenon in various GI cancers, we hypothesized that defects in ACD-NRCC could be an etiological factor in malignancy. Such a mechanism, potentially involving linking template DNA strands from multiple chromosomes to "one-side" of the mitotic plane, would be prone to "breaks" leading to aneuploidy and eventually cancer. Defects in asymmetric cell division in the drosophila results in cancer [26]. Defects in ACD-NRCC provide another explanation for how tissue stem cells initiate cancer.

A potential source of bias in our study is the use of labeled DNA nucleotides. It is conceivable that labeled-nucleotides could affect proliferation, cell cycle, cell survival, DNA replication, and cell division. However, reported data is scant, and contradictory. To test this potential source of bias, we tested cell viability/proliferation/toxicity in labeled and non-labeled cells, and found no difference in viability, proliferation and/or toxicity (figure S3D-E). Based on these data, our findings do not appear to be due to artifact (Supplemental Discussion).

We showed that ACD-NRCC is detected both in cancer cells previously described as tumor-initiating cells or putative stem-like cancer cells (Side Population and CD133+ cells), and associated with OV6 expression (A marker associated with liver progenitors). Others showed that cells undergoing ACD-NRCC express stem cells markers [9, 11], and that ACD-NRCC is not associated with differentiation markers [11]. Additionally, asymmetric cell division was

detected in intestinal stem cells [27, 28], and after tissue injury [26]. However, based on our data we cannot associate ACD-NRCC specifically or directly with cancer-stem cells or even a different cell fate [10].

Based on this work, we can't attribute ACD-NRCC exclusively to cancer stem cells. However, recently we published a paper titled '*Tumor-initiating label retaining cancer cells in human gastrointestinal cancers undergo asymmetric cell division' [14]*; in that work, we describe how some cancer cells undergoing ACD-NRCC exhibit exquisite tumor initiating capacity and multipotency gene expression profile. Moreover, there are significant differences between cells undergoing ACD-NRCC and cells undergoing SCD in terms of stem-cells and pluripotency gene expression profiles. The former exhibit stem cells and pluripotency gene expression profile with certain genes like Sox2 being expressed several hundred fold higher. In addition, we reported that the label retaining liver cancer cells are relatively resistant to the targeted cancer drug sorafenib [29]. In general, we hold the opinion that a stem-like-cancer cell is a more appropriate term. Since we can't associate directly cancer stem cells or stem-like-cancer cells with ACD-NRCC based purely on the current paper and our previous work was just recently published and was not yet validated by an independent group, we prefer to use the term "putative stem-like-cells" in the body of the text.

We found that the cancer niche can induce CD133+ cells to undergo ACD-NRCC in a paracrine fashion that does not require cell-to-cell contact. This effect could be abolished by heat denaturation of the conditioned media, suggesting a potential soluble factor. In contrast, Pine et al. found that lung CD133+ cells undergo ACD-NRCC when in direct contact with CD133- cells. One potential explanation could be that we used DNA-double-labeling and Pine et al. used single labeling (label retention). Another potential explanation could be that various cancers

(lung vs. GI cancers) respond differently to environmental signals. These observations and the potential effects of the cancer niche (microenvironment) on ACD-NRCC carry important implications to cancer and stem cells biology.

The molecular mechanism of ACD-NRCC is poorly understood. This is the first study to investigate gene expression in live cells undergoing ACD-NRCC. Cells undergoing ACD-NRCC differentially distribute TCF4 (Wnt transcription factor), up-regulate Wnt (TCF4, TCF7, CSNK2A1, and CCND2, and Sox17) and pluripotency/stem-cell (Sox2, GDF3, UTF1 and NEUROG2) genes, suggesting a stem-cell-like gene expression profile [23]. Using Ingenuity Pathway Analysis, we propose a Wnt-pluripotency pathway map for ACD-NRCC (figure S7). Most of the up-regulated genes in cells undergoing ACD-NRCC found in this study were previously reported to be oncogenes, while down-regulated genes are tumor suppressor genes [26]. Furthermore, from a mechanistic point of view, we describe the potential role that the Wnt pathway plays in ACD-NRCC. Although a Wnt agonist didn't stimulate ACD-NRCC, exposure to Wnt antagonist IWP2 and siRNA-TCF4 resulted in significant suppression of ACD-NRCC, and asymmetric distribution of TCF4. Here we show that Wnt is involved in ACD-NRCC but its precise role in the complex interactions within cells undergoing ACD-NRCC, demand further elucidation by independent groups.

Taken together, we show that subpopulations of gastrointestinal cancer cells can undergo ACD-NRCC. ACD-NRCC was detected preferentially in SP and CD133-positive cells, and was independent of cell-to-cell contact. The cancer niche, interact in a paracrine fashion, with cells undergoing ACD-NRCC, which is suppressed by Wnt antagonist and siRNA-TCF. Targeting the mechanism of ACD-NRCC might result in novel approaches for cancer therapy.

Funding: NCI grant 1ZIABC011005.

Competing interest: The authors indicate no potential conflicts of interest.

Patient consent: Obtained.

Ethics approval: Approved by NIH.

Acknowledgments: We thank Langston Lim and Poonam Annan for their excellent help in confocal microscopy.

Contributors: HWX, SST and IA conceived and designed the experiments; HWX, CA, SR, BKK, TK, GWW, DH and JEM performed the experiments; HWX, SHG, SST, IA analyzed the data; HWX, CA, KRJ, AS, UR, SST and IA wrote the paper.

REFERENCES

1. Cairns J. Mutation selection and the natural history of cancer. Nature. 1975; 255: 197-200.
2. Rando TA. The immortal strand hypothesis: segregation and reconstruction. Cell. 2007; 129: 1239-43.
3. Kiel MJ, He S, Ashkenazi R, Gentry SN, Teta M, Kushner JA, et al. Haematopoietic stem cells do not asymmetrically segregate chromosomes or retain BrdU. Nature. 2007; 449: 238-42.
4. Fei JF, Huttner WB. Nonselective sister chromatid segregation in mouse embryonic neocortical precursor cells. Cereb Cortex. 2009; 19 Suppl 1: i49-54.
5. Kuroki T, Murakami Y. Random segregation of DNA strands in epidermal basal cells. Jpn J Cancer Res. 1989; 80: 637-42.
6. Barker N, van Es JH, Kuipers J, Kujala P, van den Born M, Cozijnsen M, et al. Identification of stem cells in small intestine and colon by marker gene Lgr5. Nature. 2007; 449: 1003-7.
7. Sotiropoulou PA, Candi A, Blanpain C. The majority of multipotent epidermal stem cells do not protect their genome by asymmetrical chromosome segregation. Stem Cells. 2008; 26: 2964-73.
8. Waghmare SK, Bansal R, Lee J, Zhang YV, McDermitt DJ, Tumbar T. Quantitative proliferation dynamics and random chromosome segregation of hair follicle stem cells. The EMBO journal. 2008; 27: 1309-20.
9. Conboy MJ, Karasov AO, Rando TA. High incidence of non-random template strand segregation and asymmetric fate determination in dividing stem cells and their progeny. PLoS biology. 2007; 5: e102. doi:06-PLBI-RA-2054R2 [pii]
10.1371/journal.pbio.0050102.
10. Lansdorp PM. Immortal strands? Give me a break. Cell. 2007; 129: 1244-7.
11. Pine SR, Ryan BM, Varticovski L, Robles AI, Harris CC. Microenvironmental modulation of asymmetric cell division in human lung cancer cells. Proceedings of the National Academy of Sciences of the United States of America. 2010; 107: 2195-200.
12. Potten CS, Hume WJ, Reid P, Cairns J. The segregation of DNA in epithelial stem cells. Cell. 1978; 15: 899-906. doi:0092-8674(78)90274-X [pii].

13. Lu B, Jan LY, Jan YN. Asymmetric cell division: lessons from flies and worms. Current opinion in genetics & development. 1998; 8: 392-9.
14. Xin HW, Hari DM, Mullinax JE, Ambe CM, Koizumi T, Ray S, et al. Tumor-initiating label-retaining cancer cells in human gastrointestinal cancers undergo asymmetric cell division. Stem Cells. 2012; 30: 591-8.
15. Li F, Lu L, Lu J. Identification and location of label retaining cells in mouse liver. J Gastroenterol. 2010; 45: 113-21.
16. Cotsarelis G, Sun TT, Lavker RM. Label-retaining cells reside in the bulge area of pilosebaceous unit: implications for follicular stem cells, hair cycle, and skin carcinogenesis. Cell. 1990; 61: 1329-37. doi:0092-8674(90)90696-C [pii].
17. Potten CS, Owen G, Booth D. Intestinal stem cells protect their genome by selective segregation of template DNA strands. Journal of cell science. 2002; 115: 2381-8.
18. Smith GH. Label-retaining epithelial cells in mouse mammary gland divide asymmetrically and retain their template DNA strands. Development. 2005; 132: 681-7. doi:dev.01609 [pii]
10.1242/dev.01609.
19. Hari D, Xin HW, Jaiswal K, Wiegand G, Kim BK, Ambe C, et al. Isolation of live label-retaining cells and cells undergoing asymmetric cell division via nonrandom chromosomal cosegregation from human cancers. Stem cells and development. 2011; 20: 1649-58.
20. Haraguchi N, Utsunomiya T, Inoue H, Tanaka F, Mimori K, Barnard GF, et al. Characterization of a Side Population of Cancer Cells from Human Gastrointestinal System. Stem Cells. 2006; 24: 506-13. doi:10.1634/stemcells.2005-0282.
21. Ma S, Chan K-W, Hu L, Lee TK-W, Wo JY-H, Ng IO-L, et al. Identification and Characterization of Tumorigenic Liver Cancer Stem/Progenitor Cells. Gastroenterology. 2007; 132: 2542-56.
22. Parent R, Marion MJ, Furio L, Trepo C, Petit MA. Origin and characterization of a human bipotent liver progenitor cell line. Gastroenterology. 2004; 126: 1147-56.
23. Pera MF, Tam PP. Extrinsic regulation of pluripotent stem cells. Nature. 2010; 465: 713-20.
24. Balciunaite G, Keller MP, Balciunaite E, Piali L, Zuklys S, Mathieu YD, et al. Wnt glycoproteins regulate the expression of FoxN1, the gene defective in nude mice. Nat Immunol. 2002; 3: 1102-8.
25. Quyn AJ, Appleton PL, Carey FA, Steele RJ, Barker N, Clevers H, et al. Spindle orientation bias in gut epithelial stem cell compartments is lost in precancerous tissue. Cell stem cell. 2010; 6: 175-81.
26. Wu PS, Egger B, Brand AH. Asymmetric stem cell division: lessons from Drosophila. Semin Cell Dev Biol. 2008; 19: 283-93. doi:S1084-9521(08)00009-8 [pii]
10.1016/j.semcdb.2008.01.007.
27. Lopez-Garcia C, Klein AM, Simons BD, Winton DJ. Intestinal stem cell replacement follows a pattern of neutral drift. Science. 2010; 330: 822-5.
28. Snippert HJ, van der Flier LG, Sato T, van Es JH, van den Born M, Kroon-Veenboer C, et al. Intestinal crypt homeostasis results from neutral competition between symmetrically dividing Lgr5 stem cells. Cell. 2010; 143: 134-44.
29. Xin HW, Ambe CM, Hari DM, Wiegand GW, Miller TC, Chen JQ, et al. Label-retaining liver cancer cells are relatively resistant to sorafenib. Gut. 2013 Feb 14. [Epub ahead of print]: PMID: 23411027. .

Figures:

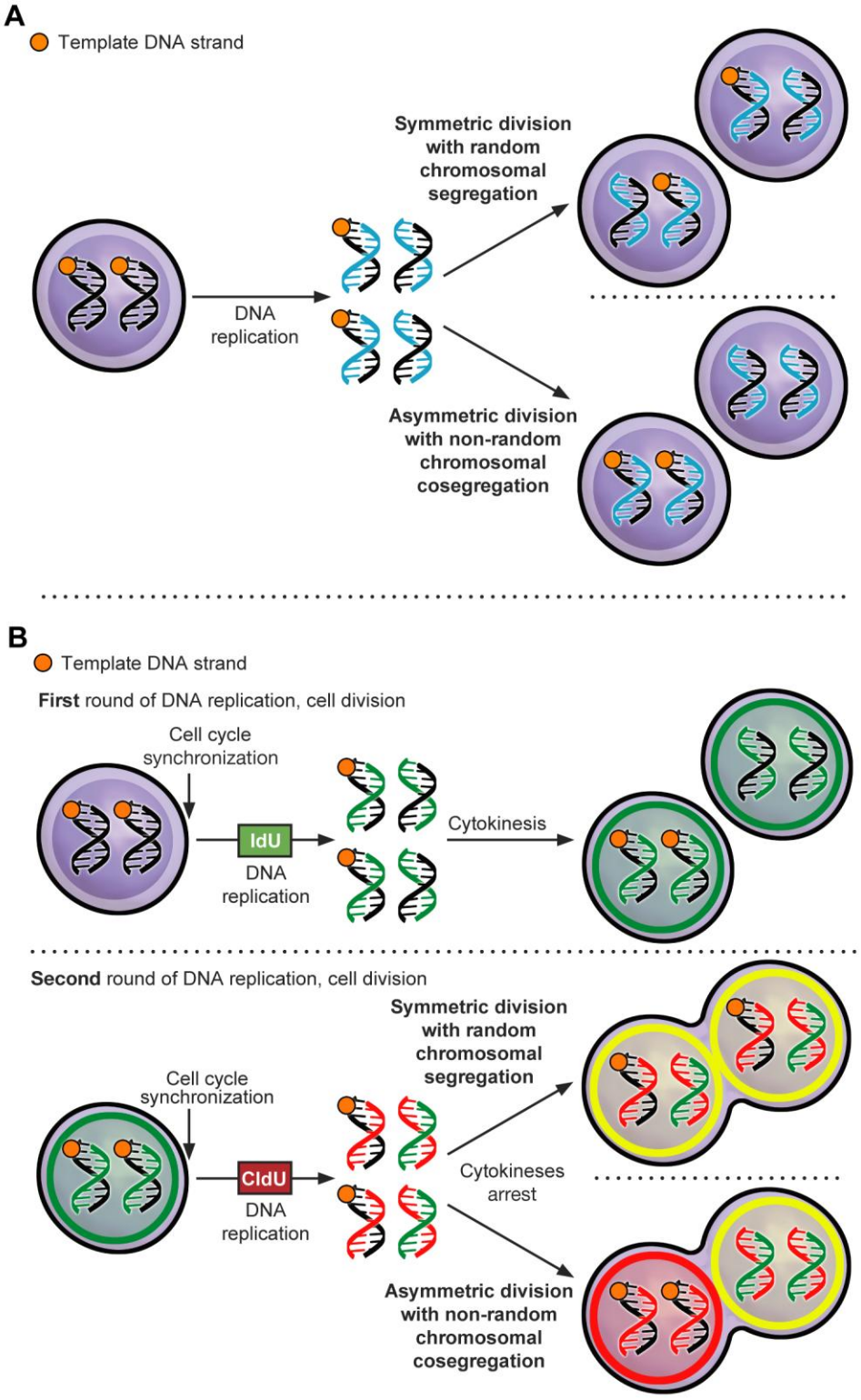
A
Template DNA strand
Symmetric division with random chromosomal segregation
DNA replication
Asymmetric division with non-random chromosomal cosegregation
B
Template DNA strand
First round of DNA replication, cell division
Cell cycle synchronization
IdU
DNA replication
Cytokinesis
Second round of DNA replication, cell division
Symmetric division with random chromosomal segregation
Cell cycle synchronization
CldU
DNA replication
Cytokineses arrest
Asymmetric division with non-random chromosomal cosegregation

Figure 1. Asymmetric cell division via non-random chromosomal cosegregation (ACD-NRCC). (A) ACD-NRCC is proposed as one potential mechanism by which stem cells self-renew. It is hypothesized that stem cells contain template DNA strands that are conserved during asymmetric cell divisions (orange). By segregating the "template DNA strands" into daughter cells destined to become stem cells, stem cells could avoid propagation of DNA replication errors. This is a potential mechanism by which mutations are preferentially segregated into daughter cells destined to differentiate and are eventually eliminated. (B) Double labeling procedure for the detection of ACD-NRCC (figure S1 and Materials and Methods; IdU (Green): Iodo-deoxyuridine; CldU (Red): Chloro-deoxyuridine).

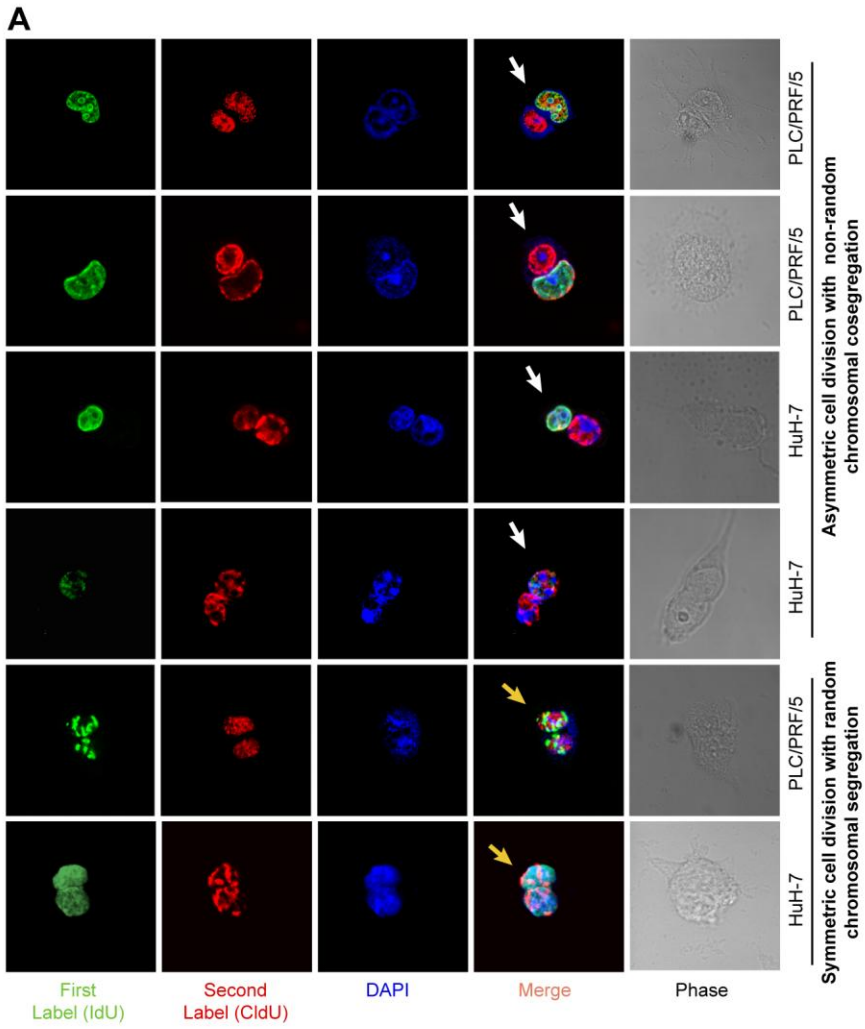
A
PLC/PRF/5
PLC/PRF/5
HuH-7
HuH-7
Asymmetric cell division with non-random chromosomal cosegregation
PLC/PRF/5
HuH-7
Symmetric cell division with random chromosomal segregation
First Label (IdU)
Second Label (CldU)
DAPI
Merge
Phase

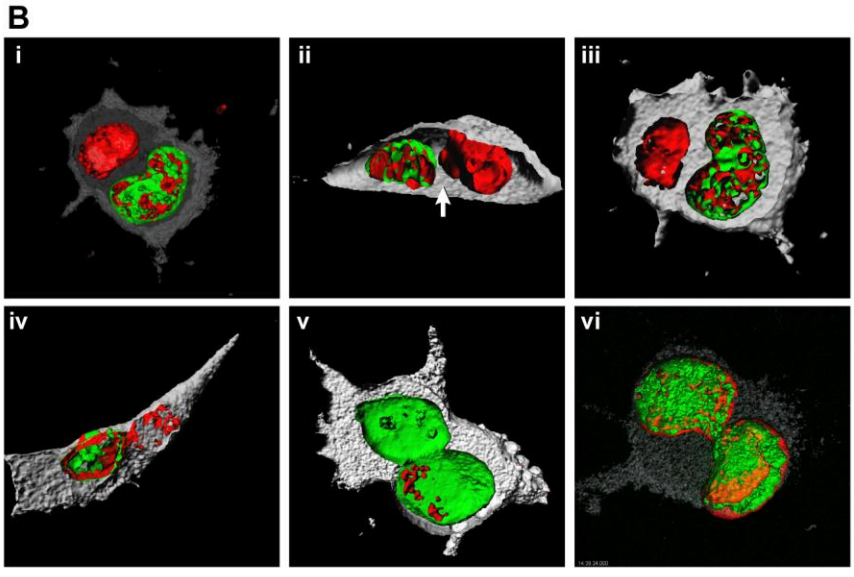
B
i
ii
iii
iv
v
vi

Figure 2. ACD-NRCC and SCD is shown in human liver cancer cells. (A) Fluorescent microscopy images showing ACD-NRCC (white arrow) and SCD with random chromosomal segregation (yellow arrow) in human liver cancers. The top four rows shows ACD-NRCC: Green fluorescent IdU is seen only in one nucleus after two cell cycles, while red fluorescent CldU is seen in both nuclei within the same cell arrested in cytokinesis. The bottom two rows show SCD, where both nuclei within one cell arrested in cytokinesis incorporated both nucleotides (figure S2). (B) Three dimensional confocal microscopy images showing human liver cancer cells and lung cancer (iv) undergoing ACD-NRCC. In (i), (ii) and (iii), we show two nuclei in the same cytoplasmic space without intervening cytoplasmic membrane during ACD-NRCC (white arrow; figure S2 and Movie S1). In (v) we show ACD-NRCC after reverse labeling. In (vi) we show SCD for comparison.

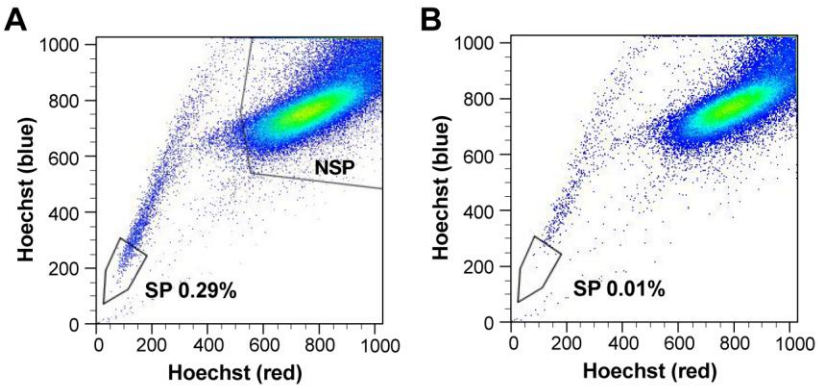

C

Week	Side population** Asymmetric cell division (% ± s.e.m.)	Non-side population** Asymmetric cell division (% ± s.e.m.)
1*	0% ± 1.0	0% ± 0
2*	1.0% ± 0.6	0% ± 0
5*	3.2% ± 1.3	0% ± 0

*p=0.0034; **p=0.024

Figure 3. ACD is detected preferentially in the Side Population of liver cancer cells. (A-B) FLOW CYTOMETRY sorting images of side population (SP) and non-side population cells (NSP). The side population is based on the ability of the ABCG2 transporter to efflux Hoechst 33342 (Ho). (B) In order to identify the population of cells that efflux Ho specifically by the ABCG2 transporter, we used Verapamil to block the activity of the ABCG2 transporter. (A) Here we show that the SP comprises 0.28% of the total cell population of Huh-7 liver cancer cells. (C) Side-population (SP) and non-SP hepatocellular carcinoma cells were plated initially at low concentrations, then allowed to proliferate, followed for 5 weeks, and tested for the presence of ACD-NRCC. At one week, SP cells did not exhibit ACD-NRCC, but when left to proliferate and differentiate while generating non-SP cells, demonstrated increasing levels of ACD-NRCC (p=0.0034); the non-SP cells neither generated SP cells nor demonstrated ACD-NRCC (p=0.024). While ACD-NRCC was never detected in NSP or CD133-negative cells (Vide Infra,

figure 4), the maximal detection rate in total cells, in SP cells or in CD133+ cells seem to be constant suggesting that per a given condition the rate of ACD-NRCC is constant (steady state rate).

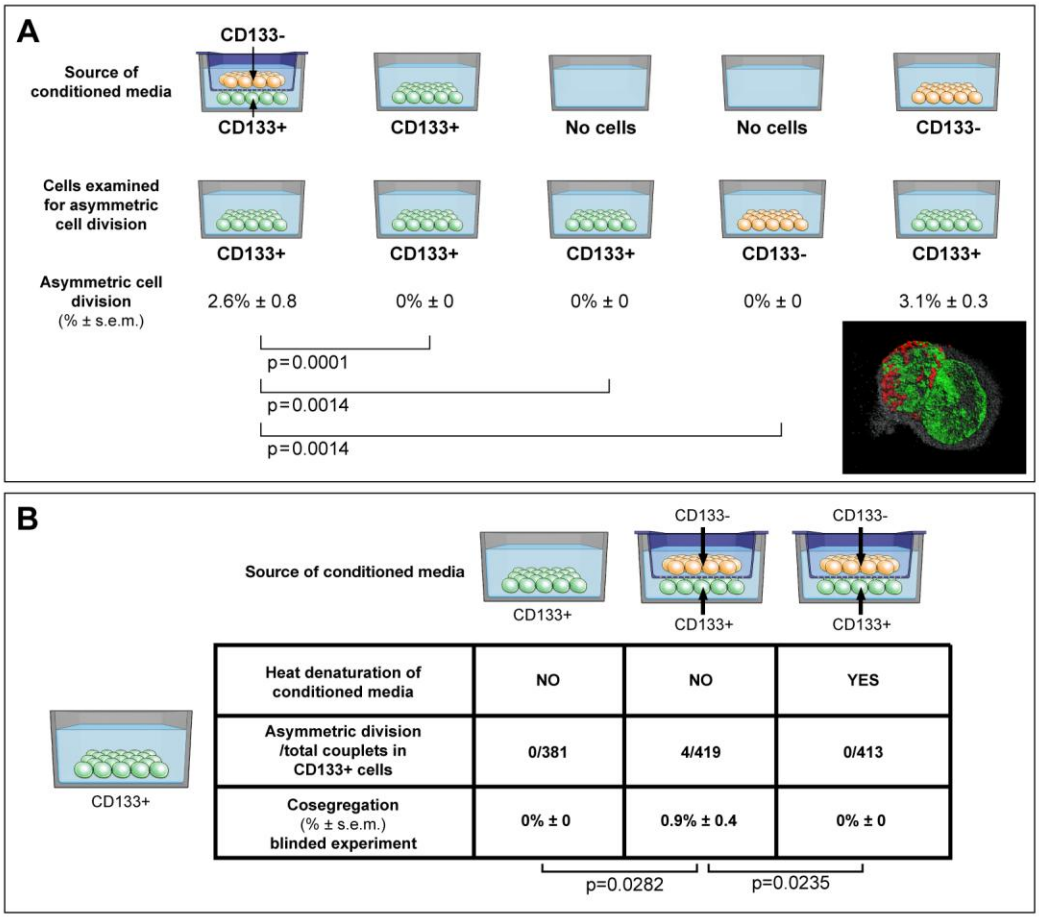

Figure 4. ACD is detected preferentially in CD133+ cells, and is modulated by the cancer microenvironment in a paracrine nature. (A) Here we show that ACD-NRCC is detected in CD133+ cells of Huh-7 liver cancer cells; no ACD-NRCC was detected in CD133-negative cells under any-condition. Additionally, we show that in order for CD133+ cells to undergo ACD-NRCC they must be cultured together with CD133-negative cells. The effect of CD133-negative cells on CD133+ cells is paracrine in nature. Thus, the effect of CD133-negative cells on CD133+ cells undergoing ACD-NRCC is not dependent on cell-to-cell contact. CD133-negative or CD133+ cells growing separately alone do not undergo ACD-NRCC. All experiments were repeated three times in a prospective blinded fashion. (B) Here we show that the permissive

effect of CD133-negative cells on CD133+ cells undergoing ACD-NRCC is heat sensitive, and can be abolished by heat denaturation. While ACD-NRCC was never detected in CD133-negative cells or NSP cells (figure 3), the maximal detection rate in total cells, in CD133+ cells or in SP cells seem to be constant suggesting that per a given condition the rate of ACD-NRCC is constant (steady state rate).

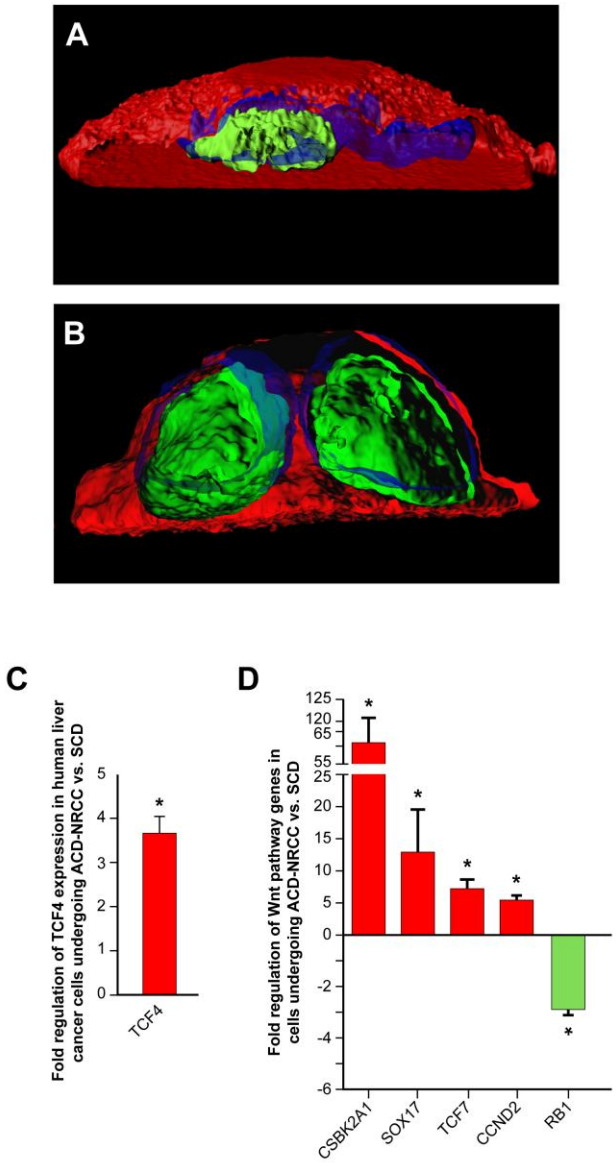

Figure 5. Wnt pathway genes are expressed asymmetrically in cells undergoing asymmetric cell division (ACD-NRCC). We studied representative Wnt associated proteins representing each of the cellular compartments (membrane, cytoplasm and nucleus). TCF4 was the only Wnt associated protein distributed asymmetrically during liver cancer cell divisions (3.1% ± 1.5%). (A) Using confocal microscopy with tridimensional rendering, we show asymmetric distribution of TCF4, and (Green=TCF4, Blue=DAPI and Red=CFSE), and (B) symmetric distribution of

TCF4. (C) We isolated live cells undergoing ACD-NRCC or SCD; using qRT-PCR, we show that TCF4 is upregulated in cells undergoing ACD-NRCC when compared to cells undergoing SCD. (D) We performed Wnt SuperArray analysis on cells undergoing ACD-NRCC or SCD. Among 84 Wnt associated genes tested only 5 were found to be differentially expressed, TCF4, TCF7, CSBK2A1 and Sox17 were upregulated, and RB1 was down-regulated by cells undergoing ACD-NRCC.

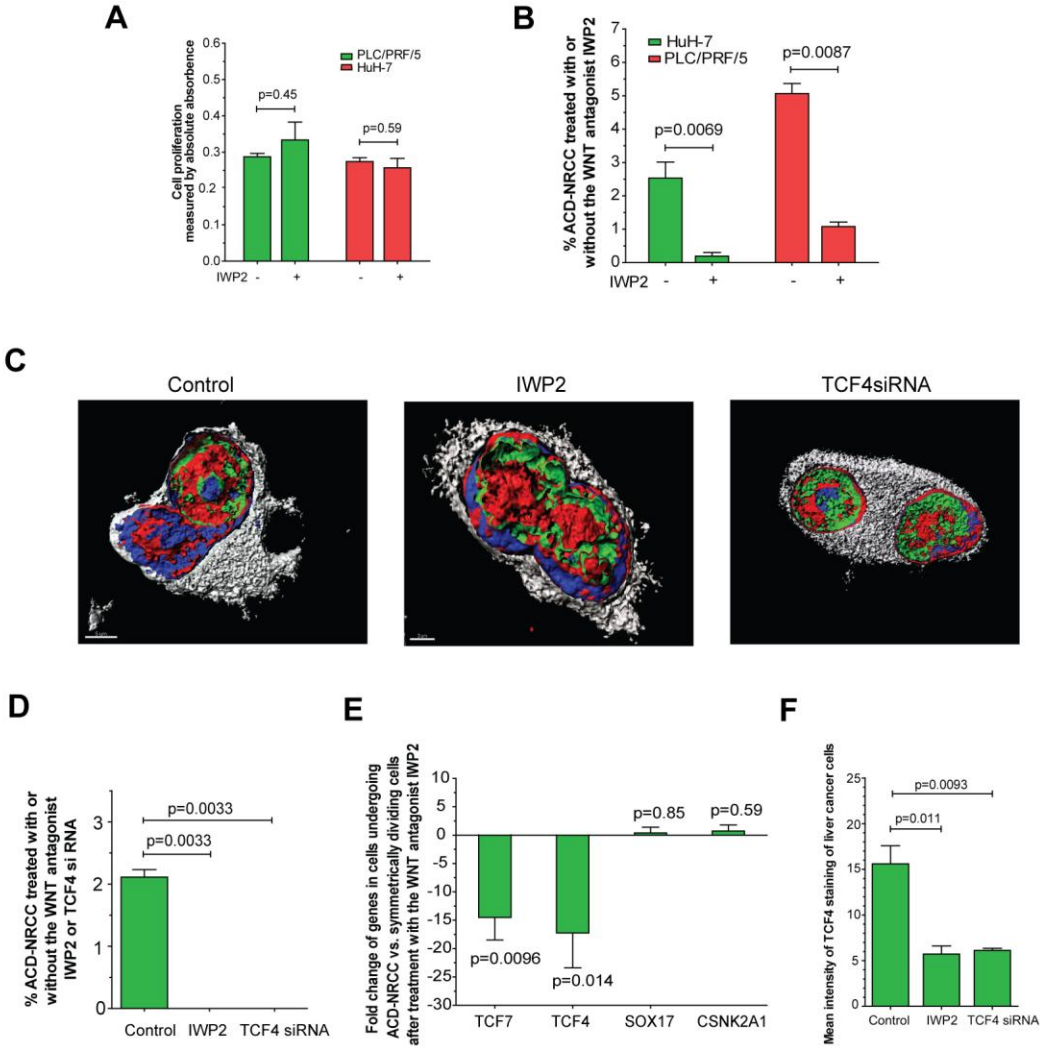

Figure 6. Inhibition of Wnt results in significant suppression of ACD-NRCC.

We detected ACD-NRCC or SCD before and after treatment with the Wnt-antagonist IWP2 or siRNA-TCF4. (A) IWP-2 didn't affect cell proliferation (0.29 ± 0.01 vs. 0.33 ± 0.0, p=0.45 for PLC/PRF/5; 0.27 ± 0.01% vs. 0.25 ± 0.03, p=0.59 for HuH-7). (B) To understand Wnt effects on ACD-NRCC in a quantitative manner, we tested for ACD-NRCC in live cells before and after 30

treatment with the Wnt-antagonist IWP2. The suppression of ACD-NRCC after treatment with the Wnt-antagonist IWP2 was statistically significant. (C-D) To further validate these results and because TCF4 was differentially expressed in cells undergoing ACD-NRCC, we tested for ACD-NRCC by confocal microscopy in fixed cells before and after treatment with the Wnt-antagonist IWP2 or TCF4-siRNA. We detected ACD-NRCC in cells before treatment with IWP2 or TCF4-siRNA. After treatment with the Wnt-antagonist IWP2 or knock down of TCF4, we couldn't detect cells undergoing ACD-NRCC; only cells undergoing SCD were observed. (E) Treatment with the Wnt-antagonist IWP2 reversed or reduced the differential expression of TCF4, TCF7, SOX17 and CSNK2A1 in cells undergoing ACD-NRCC vs. SCD (figure 5 and S5). (F) Immunofluorescence staining for TCF4 before and after treatment with IWP2 or TCF4-siRNA showed that the Wnt antagonist IWP-2 or TCF4-siRNA reduced TCF4 levels by 64% ($p=0.011$) and 61% ($p=0.0093$), respectively (figure S8).

Supplementary Material

Wnt and the Cancer Niche: Paracrine Interactions with Gastrointestinal Cancer Cells Undergoing Asymmetric Cell Division

Hong-Wu Xin[1], Chenwi M. Ambe[1], Satyajit Ray[1], Bo-Kyu Kim[1], Tomotake Koizumi[1], Gordon W. Wiegand[1], Danielle Hari[1], John E. Mullinax[1], Kshama R. Jaiswal[1], Susan H Garfield[2], Alexander Stojadinovic[3,4], Udo Rudloff[1], Snorri S Thorgeirsson[2,*], Itzhak Avital[1,4,5*]

[1]Surgery Branch, [2]Laboratory for Experimental Carcinogenesis, Center for Cancer Research, National Cancer Institute, National Institutes of Health, Bethesda, MD 20892, USA; [3]Department of Surgery, Division of Surgical Oncology, Walter Reed National Military Medical Center, [4]Department of Surgery, Uniformed Services University of the Health Sciences, Bethesda, MD; [5]Bon Secours Cancer Institute, Richmond, VA 23230, USA.

Running Title: Cancer Stem Cells, Wnt, TCF4, Label Retaining Cancer Cell, Asymmetric Cell Division, Non-random chromosomal cosegregation, cancer niche, and cancer microenvironment**.**

Correspondence:

*** Snorri S. Thorgeirsson, M.D., Ph.D.**
Head, Center of Excellence in Integrative Cancer Biology and Genomics
Chief, Laboratory of Experimental Carcinogenesis
Center for Cancer Research
National Cancer Institute, NIH
37 Convent Drive MSC 4262,
Building 37, Room 4146A,
Bethesda, MD 20892-4262, USA
Phone: 1+(301) 496-1450(O)
Phone: 1+(301) 496-1935(W)
Fax: 1+ (301) 496-0734
E-mail: snorri_thorgeirsson@nih.gov

Or

*** Itzhak Avital, MD**
Medical Director
Bon Secours Cancer Institute
Richmond, VA 23230, USA.
Email: itzhak.avital@gmail.com

Inventory of the Supplementary Material

1. **List of Supplementary Tables, Figures and Movie**

2. **Supplementary Tables**

3. **Supplementary Figure Legends**

4. **Supplementary Discussion**

5. **Supplementary Methods**

List of Supplementary Tables, Figures, and Movie

Table S1. Human cells and culture conditions used in this study

Table S2. Doubling times for all human cells tested

Table S3. Couplets detection rate with and without Cytochalasin D

Table S4. Asymmetric cell division with non-random chromosomal cosegregation: Forward and reverse labeling in liver cancer cells

Table S5. ACD-NRCC is identified in various human cancers and non-malignant liver cell line

Table S6. ACD-NRCC is identified in live human liver cancer cells using DNA double labeling technique and flow cytometry.

Table S7. ACD-NRCC is identified in live human liver cancer cells using DNA single labeling technique and flow cytometry.

Table S8. Side Population detection in tested human cancer cells

Figure S1. DNA Double labeling experimental procedure and the establishment of the experimental conditions for couplets detection

Figure S2. Three-dimensional images of cells undergoing ACD-NRCC as demonstrated by DNA dual labeling in human hepatocellular carcinoma

Figure S3. Detection and isolation of live cells undergoing ACD-NRCC: Method, Toxicity and Viability

Figure S4. OV6 a marker associated with liver progenitor cells is segregated with the template DNA strand

Figure S5. Validation of Wnt Super-array gene expression profile

Figure S6. Stem Cells SuperArray gene expression profile in cells undergoing ACD-NRCC vs. SCD

Figure S7. Stem Cell and WNT pathway analysis for cells undergoing ACD-NRCC

Figure S8. The Wnt antagonist IWP2 and isRNA-TCF4 reduced TCF4 levels but didn't affect over all cell proliferation

Figure S9. Karyotypes of human colorectal cancer cells derived from fresh surgical specimens

Movie S1. This is a movie showing three-dimensional sequential images of liver cancer cells undergoing ACD-NRCC

Tables

Table S1. Human cells and culture conditions used in this study.

Cell Source	Cell Name	Cell Source	Growth Media
Human hepatocellular carcinoma (HCC)	PLC/PRF/5	ATCC, CRL-8024	45% DMEM, 45% Ham's F-12 supplemented with 10% FCS (Invitrogen Corp, Grand Isle, NY).
HCC	HuH-7	Japan Health Sciences Foundation (JHS), JCRB0403	As for PLC/PRF/5.
HCC	SK-Hep-1	ATCC, HTB-52	As for PLC/PRF/5.
HCC	HLF	JHS, JCRB0405	As for PLC/PRF/5.
Human pancreatic cancer derived from fresh surgical specimen	Tumor cell-2596	Surgery Branch, NCI	RPMI supplemented with 15% FBS, 1% non-essential amino acids, 1% sodium pyruvate, 0.2U/ml insulin and 0.01ug/ml each of insulin-like growth factors 1&2 (Invitrogen Corp, USA).
Human pancreatic cancer	Panc-1	ATCC, CRL-1469	RPMI supplemented with 10% FCS (Invitrogen Corp, USA).
Human colon cancer	HT-29	ATCC, HTB-38	As for PLC/PRF/5.
Human melanoma derived from fresh surgical specimen	Tumor cell-526	Surgery Branch, NCI/NIH	RPMI supplemented with 10% FBS and 25mM Hepes (Invitrogen Corp, USA).
Human melanoma	SK-MEL-2	ATCC, HTB-68	As for PLC/PRF/5.
Human lung cancer	A-549	ATCC, CCL-185	As for PLC/PRF/5.
Human Benign Liver Cell	THLE-2	ATCC, CRL-2706	BEBM (CC-3171 Lonza, USA) supplemented with BEGM Singlequot Kit (Lonza, CC-4175).
Human Benign Liver Cell	THLE-3	ATCC, CRL-11233	BEBM (CC-3171 Lonza, USA) supplemented with BEGM Singlequot Kit (Lonza, CC-4175).
Human Colorectal cancer derived from fresh surgical	CSCL-01-	Developed from patient tumor in our lab	As for PLC/PRF/5.

specimen			
Human Colorectal cancer derived from fresh surgical specimen	CSCL-02-Ne	Developed from patient tumor in our lab	As for PLC/PRF/5.
Human Colorectal cancer derived from fresh surgical specimen	CSCL-03-Ba	Developed from patient tumor in our lab	As for PLC/PRF/5.
Human GI cancer of unknown origins derived from fresh surgical specimen	CSCL-04-Ke	Developed from patient tumor in our lab	RPMI supplemented with 10% FCS and 0.2U/ml insulin (Invitrogen Corp, USA).
Pancreatic adenocarcinoma	BxPC-3	ATCC, CRL-1687	RPMI supplemented with 10% FCS (Invitrogen Corp, USA).

Table S2. Doubling times for all cells tested. To effectively detect ACD, we determined the growth curves and doubling times experimentally for all cell lines and fresh tumor cells. Growth curve's correlation value $R^2 \geq 0.9$ was considered adequate for computations of doubling times.

Cell type	**Cell Name**	**Doubling times** (Hour & R^2)
Human Hepatocellular Carcinoma	PLC/PRF/5	39.7 (0.94)
Human Hepatocellular Carcinoma	HuH-7	28.9 (0.976)
Human Hepatocellular Carcinoma	SK-Hep-1	23.1 (0.976)
Human Hepatocellular Carcinoma	HLF	15 (0.957)
Human Pancreatic Cancer (Derived from fresh surgical specimen)	Tumor cell-2596	49.5 (0.905)
Human Pancreatic Cancer	Panc-1	22.4 (0.916)
Human Colon Cancer	HT-29	23.9 (0.976)
Human Melanoma (Derived from fresh surgical specimen)	Tumor cell-526	30.1 (0.998)
Human Melanoma	SK-MEL-2	43.3 (0.979)
Human Lung Cancer	A-549	18.7 (0.981)
Human Benign Liver Cell	THLE-2	40.8 (0.964)
Colorectal cancer (Derived from fresh surgical specimen)	CSCL-01-We	59.6 (0.924)
Colorectal cancer	CSCL-02-Ne	34.5 (0.962)

(Derived from fresh surgical specimen)		
Colorectal cancer	CSCL-03-Ba	30 (0.989)
(Derived from fresh surgical specimen)		
GI cancer of unknown origins	CSCL-04-Ke	20.1 (0.917)
(Derived from fresh surgical specimen)		

Table S3. Couplets detection rate with and without Cytochalasin D

Cytochalasin-D	Couplets/total cells	Couplets§ (% ± s.e.m., n=3)
+	64/107	59.9% ± 1.0
-	3/103	2.9% ± 1.7

§ p=6.1e-5

***** The rate of ACD-NRCC was determined as a percentage from total couplets and not as a % of total cells. Additionally, only couplets were counted. Therefore, it is unlikely that the results reported herein are spurious or biased. We showed that the rate of ACD-NRCC on up to 6%. The rate of spontaneous couplets is 3% but it is percentage of total cells, and not a percentage from couplets. With Cytochalasin-D the rate of couplets is 60% of total cells, and from these we detected up to 6% rate of ACD-NRCC i.e. up to 6% of 60%. Thus, also, if all the spontaneous couplets were spurious detection of ACD-NRCC it means that all these couplets had to be a fusion between a cell that did not undergo cell division (single label) and a cell that underwent two cell cycles. The likelihood for all spontaneous couplets to be of such nature is extremely low. Moreover, since we counted only couplets, to detect between up to 6% ACD-NRCC and that all these would be "spontaneous couplets" and not due to true mitosis arrest and ACD-NRCC, we would have needed approximately 10 times that amount of culture dishes. Finally, previous study where live cells undergoing ACS-NRCC were isolated demonstrated that these

cells are functionally different exhibiting pluripotency gene expression profile and exquisite tumor initiating capacity.

Table S4. Asymmetric cell division with non-random chromosomal cosegregation: Forward and reverse labeling in liver cancer cells. Forward and reverse labeling of DNA double labeling showed similar rate of ACD-NRCC, demonstrating that the detected ACD-NRCC is not caused by a bias of the DNA labels.

Labeling Order	**Asymmetric cell division/ Total couplets**	**Asymmetric cell division *** (% ± s.e.m., N=3)
IdU-CldU	6/95	6.3% ± 0.1
CldU-IdU	7/114	6.0% ± 2.0

Table S5. ACD-NRCC is identified in various human cancers and non-malignant liver cell line

Cell source	Cell name	Asymmetric cell division/total couplets	Asymmetric cell division§ (% ± s.e.m.)
Hepatocellular carcinoma	PLC/PRF/5	22/815	2.6% ± 0.6
Hepatocellular carcinoma	HuH-7	5/514	0.9% ± 0.4
	HuH-7	6/95	6.3% ± 0.1
Hepatocellular carcinoma	SK-Hep-1	4/301	1.3% ± 0.3
Pancreatic cancer (fresh surgical specimen)	Tumor cell-2596	1/100	1.0% ± 1.0
Melanoma (fresh surgical specimen)	Tumor cell-526	3/301	1.0% ± 0.01
Lung cancer	A-549	7/298	2.3% ± 0.3
Benign human liver cells	THLE-2	4/305	1.3% ± 0.3

Table S6. ACD-NRCC is identified in live human liver cancer cells using DNA double labeling technique and flow cytometry.

Cell source	Cell name	Asymmetric cell division§ (% ± s.e.ma.)	Cells undergoing ACD-NRCC (Live cells isolated by flow cytometry)
Hepatocellular carcinoma	PLC/PRF/5	5.1% ± 0.3	14500/284,314
Hepatocellular carcinoma	HuH-7	1.5% ± 0.2	11130/742,000

Table S7. ACD-NRCC is identified in live human liver cancer cells using DNA single labeling technique and flow cytometry.

Cell source	Cell name	LRCC/ Total cells (Flow cytometry analysis only)	% LRCC (% ± s.e.m)	LRCC (Total number of live cells isolated by flow cytometry)
Hepatocellular carcinoma (HCC)	PLC/PRF/5	625/41667	1.5 ± 0.07	1e6
HCC	HuH-7	592/12639	2.6 ± 0.2	1e6
HCC	SK-Hep-1	308/34222	0.9 ± 0.01	1.1e6
Benign liver cells	THLE-2	3154/70534	3.6 ± 0.1	1e5
Benign liver cells	THLE-3	1225/40550	2.6 ± 0.6	3e4
Colorectal cancer (Fresh surgical specimen)	CSCL-01-We	537/47556	0.7 ± 0.04	5.2e3
Colorectal cancer (Fresh surgical specimen)	CSCL-02-Ne	123/64928	0.1 ± 0.02	3.9e5
Colorectal cancer (Fresh surgical specimen)	CSCL-03-Ba	13791/866007	1.7 ± 0.2	2.6e4
GI cancer of unknown origins (Fresh surgical specimen)	CSCL-04-Ke	328/83763	0.6	3.1e5

Pancreatic adenocarcinoma	Panc-1	712/14183	5.0	3.2e5
Pancreatic adenocarcinoma	BxPC-3	822/17269	4.8	1e6

Table S8. Side Population was detected in tested human cancer cells.

Cell	Side population (% ± s.e.m., N=3)
HuH-7	0.31 ± 0.03
Pan-1	5.23 ± 1.74
SK-MEL-2	1.17 ± 0.92
HT-29	5.8

Supplementary Figures

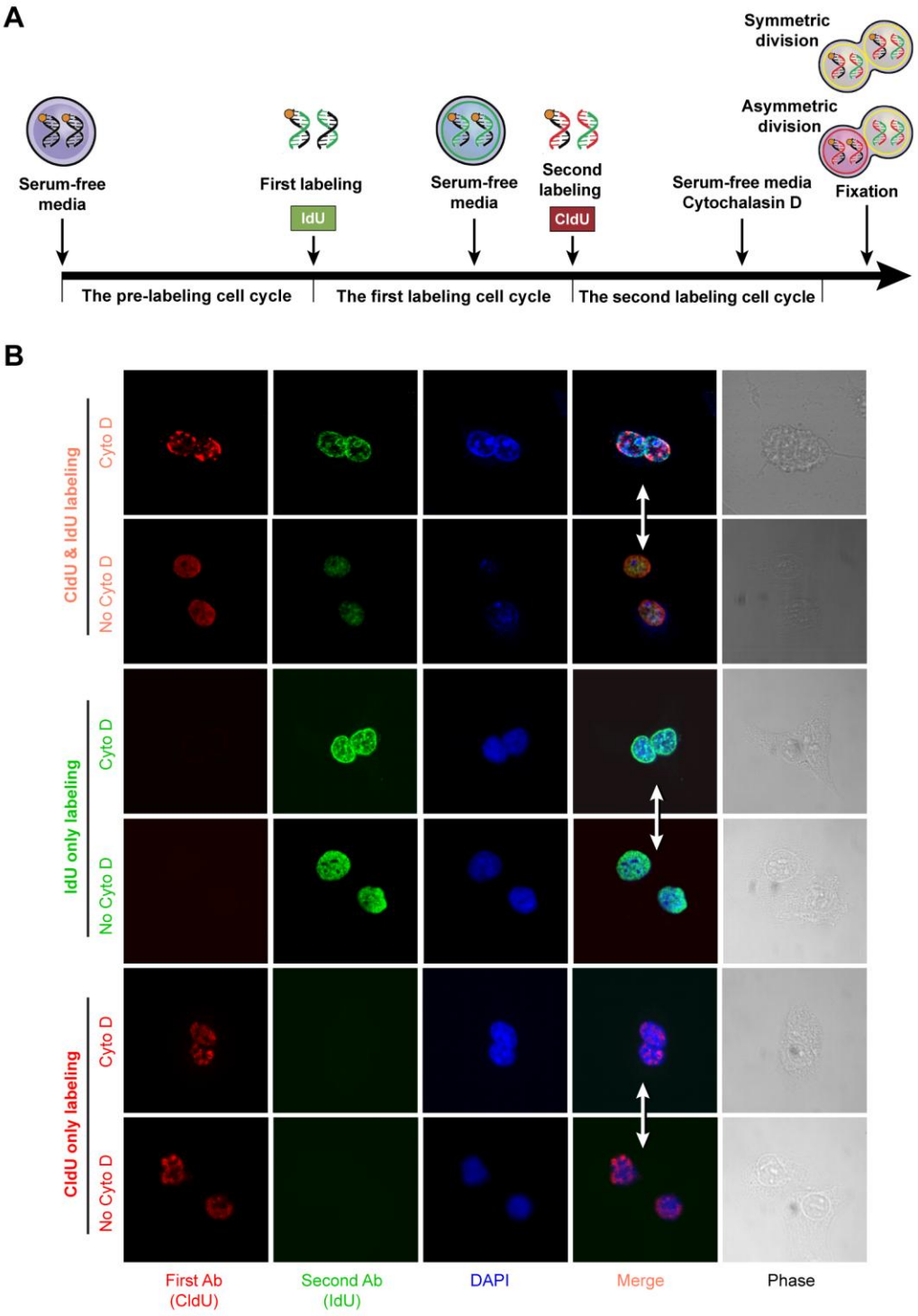

Figure S1. DNA Double labeling experimental procedure and the establishment of the experimental conditions for the detection of couplets. (A) Double labeling procedure for detection of asymmetric cell division with non-random chromosomal cosegregation (ACD-NRCC) Schema. According to the cell doubling times determined (table S2), cells were first synchronized in serum-free media (SFM) for one cell doubling time. This was done in order to have optimal number of cells at the G1/G0 phase before the initiation of the double labeling experiment. For the first DNA replication cycle, cells were labeled with the first thymidine analog either IdU or CldU in complete growth media. Before the start of the second DNA replication cycle, growth media were replaced with SFM again. At the completion of the first cell cycle, cells were trypsinized and plated singly in collagen IV-coated 8-well chamber slides (Ibidi, Germany) in complete growth media containing the second thymidine analog either CldU or IdU. Before the completion of the second cell cycle, growth media were replaced with SFM containing Cytochalasin- D (2 μM final concentration, Sigma) to arrest cells at cytokinesis. (B) To test for the possibility that these results are not due to cell fusion, CldU and IdU labeling was done with and without Cytochalasin D. Arresting cells at cytokinesis allowed us to observe cells before complete cell division. Arrested cells appeared as couplets. This methodology avoids confusion with the appearance of couplets that theoretically could have been a product of cell fusion. In addition, cells were plated singly to avoid attachment to each other. Extensive control experiments were performed with and without Cytochalasin D demonstrating that the observed asymmetric cell division was not spurious observation due to cell fusion or because cells were attached to each other (white double arrow). The effects of cytokinesis arrest by Cytochalasin D are shown here.

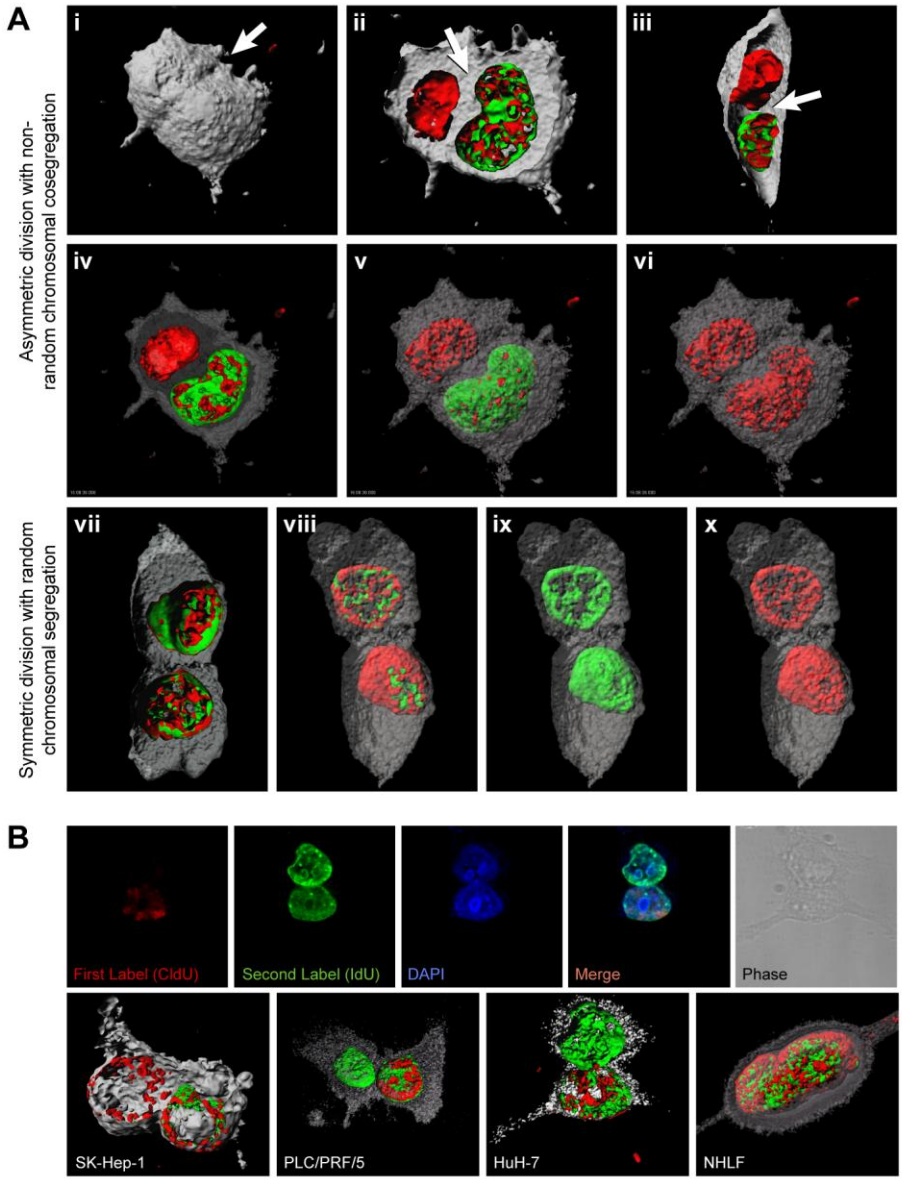

Figure S2. Three-dimensional images of cells undergoing ACD-NRCC as demonstrated by DNA dual labeling in human hepatocellular carcinoma.

(A) Forward labeling. (i-vi) and SCD with random chromosomal segregation (vii-x) in human hepatocellular carcinoma cells, PLC/PRF/5 are shown. (i-iii) These three dimensional images of a cell undergoing asymmetric division with non-random chromosomal cosegregation showing that the cell just started to divide but is now in cytokinesis arrest with a continuous cytoplasmic

membrane at the division plan (the white arrow in i). The cytoplasmic membrane can be seen in the periphery of the cell (ii and iii), but there is no intervening membrane between the two nuclei (white arrows in ii and iii), demonstrating that the two nuclei are in the same cytoplasmic space. (iv-x), Using photo-image layering, these photomicrographs demonstrate the distribution and incorporation of the two fluorescent-tagged-nucleotides. The layering was performed to show that one dye does not hinder identification of the other when both are incorporated. (B) Reverse labeling. Previous photomicrographs have demonstrated asymmetric cell division with non-random chromosomal cosegregation using IdU (Green) as the first labeled nucleotide and CldU (Red) as the second labeled nucleotide. To test whether the two differently modified nucleotides might affect the experimental results, we used reverse labeling. Asymmetric cell division rate after reverse labeling (CldU-IdU) did not differ statistically from forward labeling (IdU-CldU), as demonstrated in table S4. (Top lane) Fluorescent confocal microscopy images of human liver cancer cells undergoing asymmetric cell division (reverse labeling). After asymmetric cell division the first labeled nucleotide (CldU, red) is retained in only one nucleus while the second nucleotide (IdU, green) is retained in both. (Bottom lane) Confocal microscopy with three dimensional images showing asymmetric division after forward labeling (IdU-CldU, SK-Hep-1), and reverse labeling (CldU-IdU) in two different human liver cancer cells PLC/PRF/5 and Huh-7; and SCD in normal human lung fibroblast (NHLF).

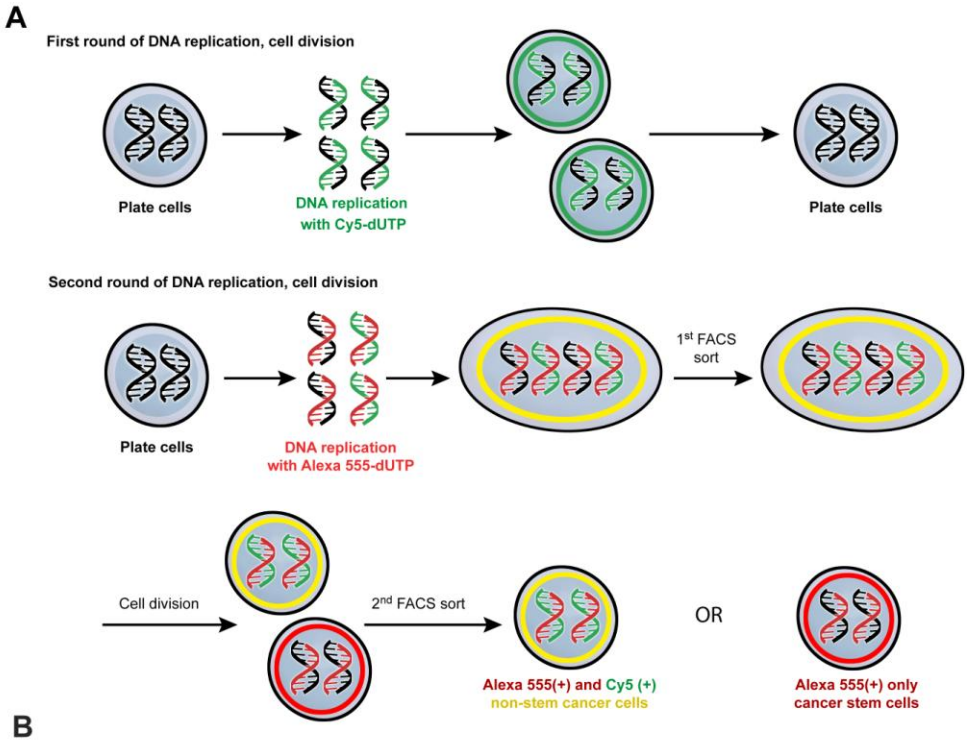
A
First round of DNA replication, cell division
Plate cells
DNA replication
with Cy5-dUTP
Plate cells
Second round of DNA replication, cell division
Plate cells
DNA replication
with Alexa 555-dUTP
1st FACS
sort
Cell division
2nd FACS sort
Alexa 555(+) and Cy5 (+)
non-stem cancer cells
OR
Alexa 555(+) only
cancer stem cells

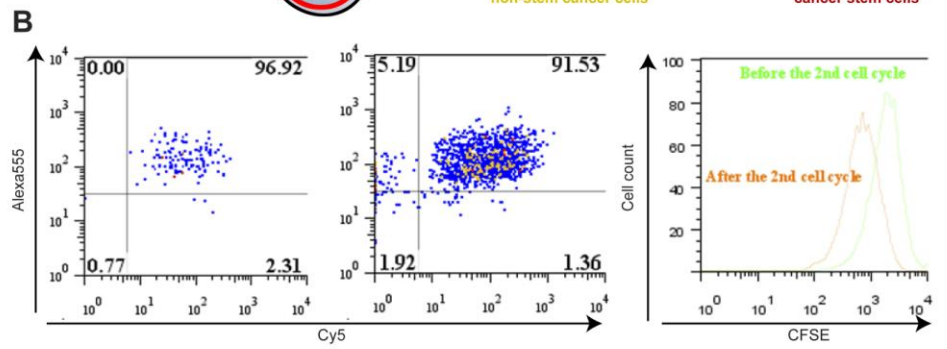
B
0.00
96.92
0.77
2.31
5.19
91.53
1.92
1.36
Alexa555
Cy5
Before the 2nd cell cycle
After the 2nd cell cycle
Cell count
CFSE

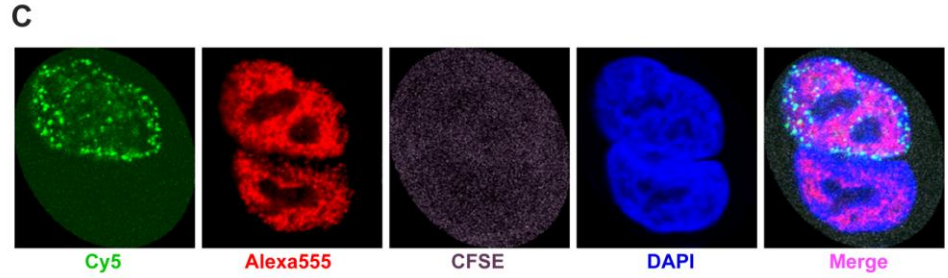
C
Cy5
Alexa555
CFSE
DAPI
Merge

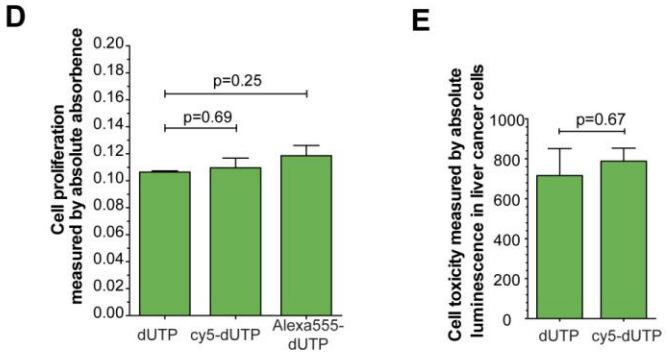
D
Cell proliferation
measured by absolute absorbence
p=0.25
p=0.69
dUTP
cy5-dUTP
Alexa555-
dUTP

E
Cell toxicity measured by absolute
luminescence in liver cancer cells
p=0.67
dUTP
cy5-dUTP

Figure S3. Detection and isolation of live cells undergoing ACD-NRCC: Method, Toxicity and Viability (A) The experimental procedures for the isolation of live cells undergoing ACD-NRCC: For the first cell cycle of DNA replication, liver cancer cells were plated, labeled with Cy5-dUTP (green) and were let to complete the first cell division in culture. Cell cycle was monitored using CFSE. Subsequently, cells that completed the first round of DNA replication were labeled with Alexa555 (red). Prior to completion of the second round of DNA replication, cells that were Alexa555-high/Cy5-high were sorted by FLOW CYTPMETRY, and placed in a culture to complete mitosis. At the completion of mitosis of the second round of DNA replication, cells that underwent exactly two cell divisions (monitored by CFSE) were analyzed and subsequently sorted. The cultured cells that previously contained only Alexa555-high/Cy5-high cells now generated two populations of cells: Alexa555-high/Cy5-high cells generated by SCD and Alexa555-high only i.e. cells generated by ACD-NRCC. CFSE was used to detect contemporaneously cell division status. (B) Typical flow cytometry dot-plots of cells undergoing ACD-NRCC using the double labeling technique in live cells. After DNA double labeling, and before the completion of the second cell division, we sorted Cy5+/Alexa555+ cells (see also A above). Nota bene, there were no Cy5-/Alexa555+ cells (the left most dot-plot) before completion of the second cell division. After completion of the second mitosis, the doubly labeled Cy5+/Alexa555+ cells generated double-labeled cells and the singly labeled Cy5-/Alexa555+ cells (5.19%, middle dot-plot). The right most histogram show that only cells that underwent two, and only two cell divisions, were sorted and analyzed, as indicated by CFSE indicator. (C) Three dimensional fluorescent confocal microscopy capturing asymmetric cell division in live cells: To confirm the results described above, we tested the products of the cell sorting after each stage. Live cell undergoing ACD-NRCC is illustrated containing one nucleus

with the 2nd labeled nucleotides only (green) and the other nucleus containing both nucleotides (green and red). The DAPI (blue) reveals two nuclei within the same cytoplasmic space halted at cytokinesis. (D) We measured cell proliferation (Supplementary Methods) to test for potential toxicity induced by the labeled nucleotides. There were no statistically significant differences in terms of proliferative capacity between cells labeled with Cy-5-dUTP, Alexa-555-dUTP or dUTP (control). (E) We measured cell toxicity (Supplementary Methods) to test for potential toxicity induced by the labeled nucleotides. There were no statistically significant differences in toxicity between cells labeled with Cy-5-dUTP or dUTP (control).

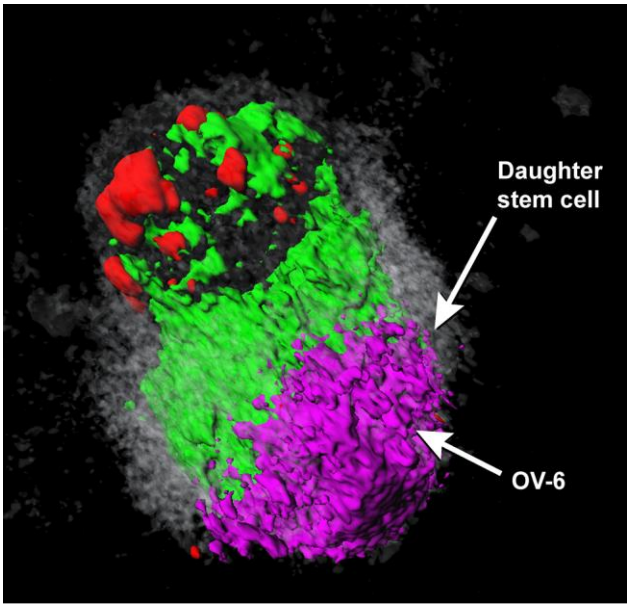

Figure S4. OV6 a marker associated with liver progenitor cells is segregated with the template DNA strand. This is a three-dimensional image showing liver cancer cell undergoing asymmetric cell division with non-random chromosomal cosegregation (ACD-NRCC). Additionally, we show that OV6 (Magenta), a marker associated with liver stem cells, is segregated asymmetrically with the template DNA strand

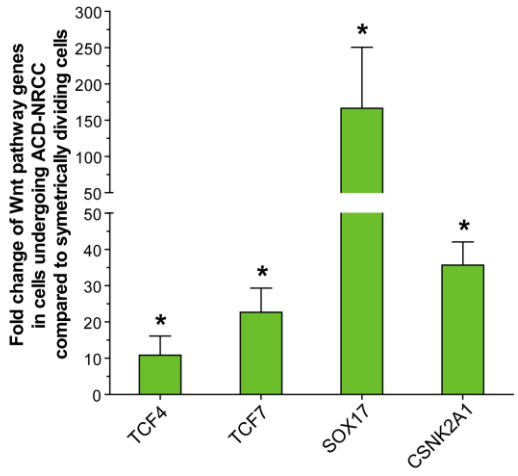

Figure S5. Validation of Wnt Super-array gene expression profile. To validate array data, we performed real-time qRT-PCR for individual Wnt genes found to be differentially expressed using Wnt Super-array. The upregulation of the four Wnt genes previously found in cells undergoing ACD-NRCC was validated using independent qRT-PCR (TCF4, TCF7, CSBK2A1 and Sox17).

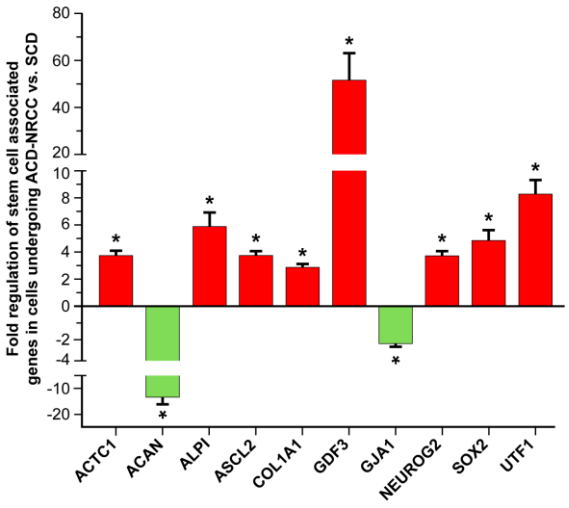

Figure S6. Stem Cells SuperArray gene expression profile in cells undergoing ACD-NRCC vs. SCD. To further understand the potential stem-like nature of cells undergoing ACD-NRCC, we used our recently developed method to isolate live cells undergoing ACD-NRCC and SCD from several HCC cell lines. We performed SuperArray analysis using stem cell gene expression platform. We tested 84 stem cells associated genes, eight genes were up-regulated in cells undergoing ACD-NRCC vs. cells undergoing SCD: GDF3, a key pluripotency growth signal and differentiation factor 3, 49.2 ± 11.1 folds, p=0.049 [1]; Sox2 a key pluripotency transcription factor (SRY, sex determining region Y-box 2), 4.7 ± 0.8 folds, p=0.05 [1]; UTF1 a pluripotency transcription factor (undifferentiated embryonic cell transcription factor 1), 8.31 ± 1.02 folds, p=0.05 [2]; Neurogenin-2 a neural stem cell markers (Neurog2), 7.0 ± 0.6, p=0.020; ASCL2 (Achaete-scute complex homolog 2), 3.8 ± 0.3, p=0.023; ACTC1 a lineage gene encoding structural proteins, 3.8 ± 0.3, p=0.023; ALPI an intestinal alkaline phosphatase, 5.94 ± 0.98, p=0.015; and COL1A1 (collagen type I alpha 1), 2.9 ± 0.2, p=0.001. Two cell adhesion genes were down-regulated: ACAN (aggrecan), 13.35 ± 2.54, p=0.042; and GJA1 (gap junction protein

alpha 1), 2.7 ± 0.2, p=0.0001). These data show that cells undergoing ACD-NRCC upregulate certain pluripotency genes associated with a potential stem cell gene expression profile.

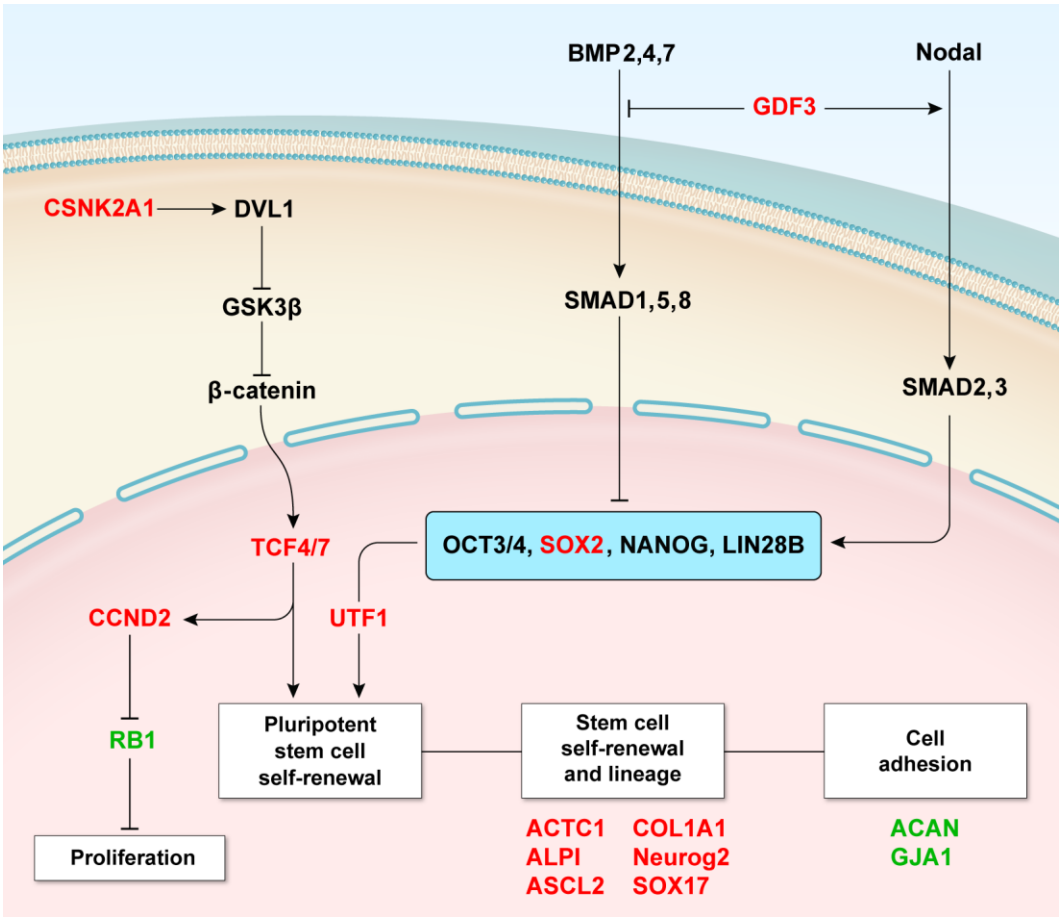

Figure S7. Stem Cell and WNT pathway analysis for cells undergoing ACD-NRCC. To further understand the possible interactions of the genes identified in cells undergoing ACD-NRCC, we analyzed the gene expression data using Ingenuity Pathway Analysis (IPA) software and proposed a possible molecular pathway map for cells undergoing ACD-NRCC. These data show that cells undergoing ACD-NRCC upregulate certain pluripotency genes associated with a stem cell gene expression profile.

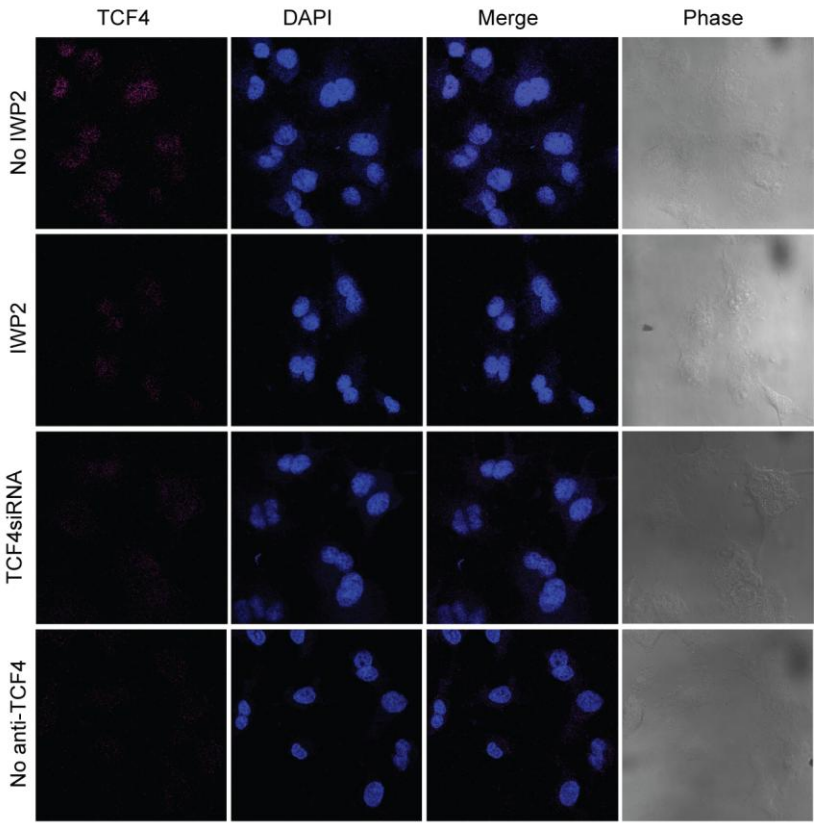

Figure S8. The Wnt antagonist IWP2 or TCF4-siRNA reduced TCF4 level without affecting cell proliferation. This is immunofluorescence staining for TCF4 before and after treatment with IWP2 or TCF4-siRNA. To accurately determine the staining intensity levels of TCF4 expression, we used the LSM ImageBrowser 4.0 (supplementary Methods). The Wnt antagonist IWP-2 or isRNA-TCF4 reduced TCF4 levels by 64% (p=0.011) and 61%, respectively (figure 6F).

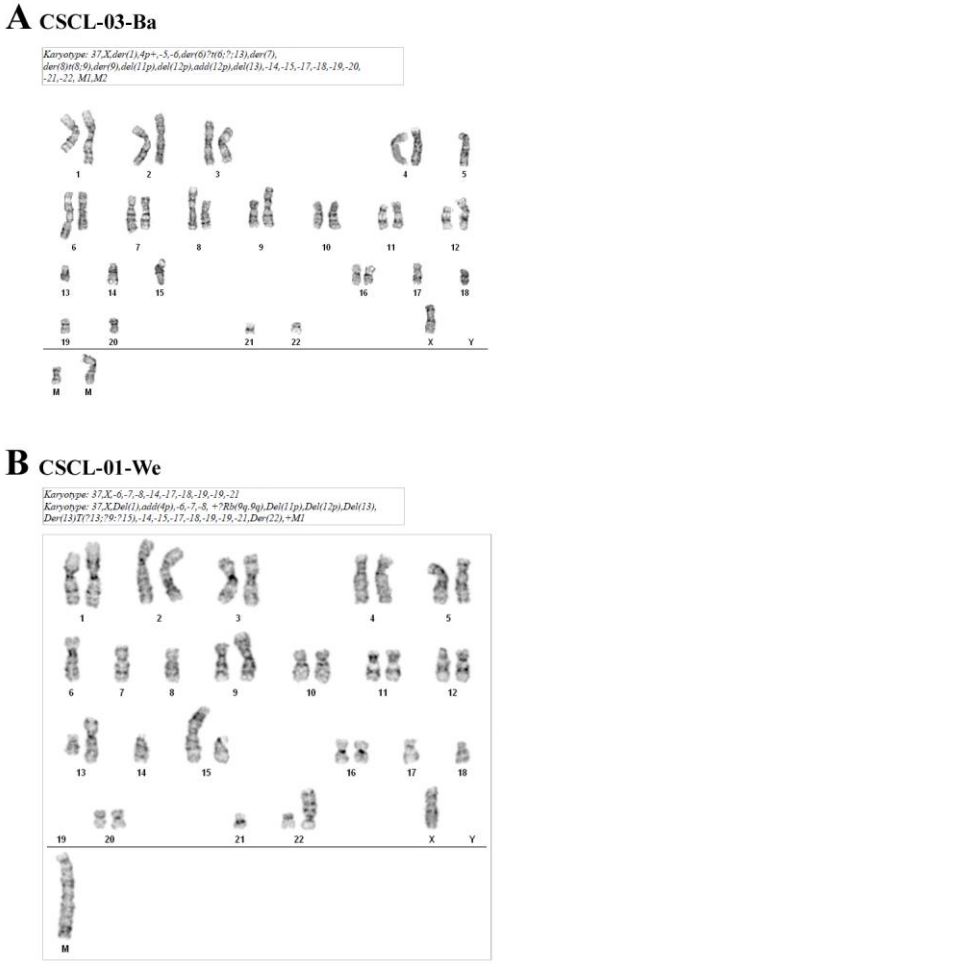

Figure S9. Karyotypes of human colorectal cancer cells derived from fresh surgical specimens. To test for potential interactions between ACD-NRCC and the Karyotype, we karyotyped two human colorectal cancer cells derived from fresh surgical specimens. Their chromosome numbers were 37 and 37 for CSCL-03-Ba (A) and CSCL-01-We (B), respectively. We couldn't clearly determine whether an interaction exist between the Karyotype of a cell and the ability to detect or differences in rate of ACD-NRCC between the various karyotypes.

Supplementary Discussion

The apparently low frequency of cells undergoing ACD-NRCC

We would like to discuss several points in this regard: It is possible that biologically the frequencies of ACD-NRCC are indeed intended to be low i.e. if one hypothesizes that ACD-NRCC are a component of self-renewal (not necessarily an exclusive component), or better stated one of several possible self-renewal divisions mechanisms than it is possible that the true frequency of ACD-NRCC is low. Clearly, more work needs to be done defining the results of ACD-NRCC in terms of self-renewal, which is beyond the scope of this paper. Two important questions in this regard are: How many cells need to undergo self-renewal divisions at any give time period, and under what conditions? These two questions deserve another study that we plan to initiate in the near future. However, this hypothesis and subsequent questions require a different line of investigation and was not part of this manuscript.

The second point is that although the frequency of ACD-NRCC is low, it is statistically significant. We worked extensively with our biostatistics department to explore mathematically this question. In summary: The theoretical probability of detecting a single cell that underwent ACD-NRCC would be extremely small (one-in-2^{23} cell divisions), <<<0.00001 for any given experiment. For any given experiment in which one or more ACD-NRCC are identified, the two-tailed p-value for the exact binomial test of whether the observed fraction is equal to any value of 0.00001 or less is <0.0001. Thus, any instances in which at least a single ACD-NRCC would be identified in an experiment would be extremely unlikely to occur by chance.

Third, we tested non-malignant liver cells (THLE-2 and THLE-3) for ACD-NRCC. We found that non-malignant liver cells undergo ACD-NRCC at a rate of 1.3% ± 0.3 (THLE-2), and 2.6 ± 0.6% (THLE-3). Identifying ACD-NRCC at similar rates both in malignant and non-malignant cells suggest that it is possible that at these conditions (normal culture conditions) the rate of ACD-NRCC is somewhat constant. Again, if one accepts that ACD-NRCC can represent self-renewal, it makes sense that under normal conditions only a fixed number of cells need undergo self-renewal. Detecting ACD-NRCC in non-malignant cells further supports the existence of ACD-NRCC in gastrointestinal cancer cells.

To address the question regarding the low numbers and the possibility of rare events being an artifact, we performed additional experiments. We tested ACD-NRCC using two alternative methods. The first method involves isolation of live cells that underwent ACD-NRCC after double labeling using flow cytometry. The second method involves isolating cell that underwent ACD-NRCC after single labeling (label retaining cancer cells, LRCC) using flow cytometry [3, 4]. Using flow cytometry and not manual cell counting afforded us counting more total cells, and more cells undergoing ACD-NRCC. In certain experiments we detected over a million cells undergoing ACD-NRCC, and over all we detected over 5 million cells undergoing ACD-NRCC in 11 deferent histologies. We suggest that in spite the low frequency, identifying over a million cells undergoing ACD-NRCC per specific experiment and detecting ACD-NRCC both in cancer and non-malignant cells further strengthen and support our findings.

First, we further tested ACD-NRCC in 4 additional cell lines using the in-situ florescence method SK-Hep-1 (liver cancer), A-549 (lung cancer), Tumor cell-526 (Melanoma), and THLE-2 (non-malignant liver cell line). We decided to perform 3 experiments per cell line;

in each of the experiments, we a priori decided to counts 100 couplets for a total of 300 couplets for each of the cell lines. We found that the rates of ACD-NRCC were 1.3% ± 0.3, 2.3% ± 0.3, 1.0% ± 0.01, and 1.3% ± 0.3, respectively (table S5). Total cells counts were 2634, total cells undergoing ACD-NRCC were 46 i.e. 46/2634=1.7%. Detecting ACD-NRCC in additional 3 cancer cell lines and one non-malignant cell line support our previous findings.

Second, to further overcome the low numbers issue, we used flow cytometry to isolate live cells undergoing ACD-NRCC using double labeling based method [3, 4]. Using this method, we detected 25,630 live cells undergoing ACD-NRCC out of 1026314 cells (PLC/PRF/5 14500 cells, and HuH-7 11130 cells; table S6). This experiment was done independently using two liver cancer cell lines PLC/PRF/5 and HuH7.

Third, to further validate that the observed ACD-NRCC is not an artifact, we used the single labeling method to isolate live cells undergoing ACD-NRCC by flow cytometry. Previously, we have demonstrated that LRCC (label retaining cancer cells) undergo ACD-NRCC; among several lines of evidence, we showed a movie demonstrating in real time live cells undergoing label retention asymmetric cell division with non-random chromosomal cosegregation[3, 4]. We used 3 additional liver cancer cell lines in 9 different experiments. Overall, we detected and isolated over 5 million cells from 11 different histologies in 31 different experiments: 3 liver cancers, 2 non-malignant liver cells, 2 pancreatic cancers and 4 colorectal cancer cells generated from 4 different fresh surgical specimens (table S7).

The potential bias introduced by halogenated-nucleotides

Because significant amount of scientific work, across several fields is based on usage of BrdU, CldU and IdU, several investigators investigated the effects of halogenated nucleotides

incorporation on cell proliferation, survival and DNA replication. Prior to embarking onto this project, we reviewed the available literature and tested several hypotheses in this regard in our laboratory.

Among several concerns, there are 3 cardinal concerns regarding halogenated-nucleotide as related to this project. One, do halogenated-nucleotides affects proliferation and the cell cycle; two, do they affect cell survival; and three, do they affect DNA replication-chromosomal segregation and/or cell division. Careful examination of the literature reveals that the data is scant and variable. Several reasons can account to the great variability and heterogeneity: The variety of cells used, animals of origins, cancer vs. non-cancer cells, and most importantly the conditions tested and the concentrations of the halogenated-nucleotides used. Thus we tested these three questions in our laboratory here and in previous work done on ACD-NRCC [3, 4].

We tested cell viability/proliferation using the Dojindo Kit (Supporting Methods). Technology for the isolation of live cells undergoing ACD-NRCC using CldU ad IdU is not available, and testing proliferation/viability on the whole population of cells will not answer the question specifically concerning labeled cells undergoing ACD-NRCC. Thus we tested cells labeled with Cy-5-dUTP and Alexa-555-dUTP undergoing ACD-NRCC (cells used in large quantities in our experiments to demonstrate ACD-NRCC). We show that there is no statistically significant difference in the proliferative activity of cells exposed to equimolar concentrations of dUTP, or the halogenated nucleotides Cy5-dUTP and Alexa-555-dUTP (figure S3D). Next, we tested the cell cycle phases and composition in various cell lines in cells exposed to non-halogenated nucleotides (dUTP), and the halogenated nucleotides. Additionally, we did not find differences between labeled cells to non-labeled cells in terms of doubling times [4]. We did not find significant differences in terms of the cell cycle between cells exposed to labeled-

nucleotides (55.3% ± 3.9, 20.3% ± 5.4 and 16.9% ± 3.4 are in G1/G0, S and G2/M phase) vs. control cells (p=0.21, p=0.59 and p=0.28, respectively; 3 different cell lines, N=9). Other investigators reported on similar findings i.e. no significant effects induced by halogenated-nucleotides on cell proliferation and cell cycle; albeit tests were done on whole cells and not cells undergoing ACD-NRCC specifically [5, 6].

Cortes et al. investigated the effects of halogenated-nucleotides on DNA replication and cell division [7, 8]. The authors discovered that halogenated-nucleotides could induce endoreduplication. This phenomenon was directly related to the concentration of halogenated-nucleotides and on Topoisomerase-II. Cortes et al. used 5 times the concentration of halogenated nucleotides that we used in our protocols; a fact that according to Cortes et al. could reduce the occurrence of endoreduplication significantly. Cortes et al. used a hamster Topoisomerase-II, and we used human cells. Since endoreduplication is directly related to the way that Topoisomerase-II interacts with halogenated-nucleotides, we can't ascertain that the same phenomenon would be observed with human Topoisomerase. The most significant difference is the method used to detect endoreduplication. First, to detect endoreduplication Cortes et al. reported that one must expose cells to halogenated-nucleotides for two S phases. It indicates that endoreduplication doesn't apply to our observations regarding LRCC, as we expose cells for only one cell cycle and follow cells for up to 18 generations. Second, Cortes et al. used a nuclear preparation to detect endoreduplication while we used cells that are actually halted during mitosis. In fact, if one examine a paper from the same group published in 2006 one can see that endoreduplication is unlikely to account for the observation of ACD-NRCC as endoreduplication is a fatal event and generate one nucleus per cell while we detected two nuclei both having labeled DNA. Lastly, to detect endoreduplication, one needs to expose cells to halogenated-nucleotides for two

consecutive cell cycles but the detection is done after cells are recovered for one more third S-phase; we detect ACD-NRCC after the second and before the third S-phase. As in endoreduplication one detects both nucleotides, and in ACD-NRCC one detects cell with two nuclei where one nucleus have only one of two species of halogenated-nucleotides. Detection of endoreduplication using our method would result in cell with one nucleus. Finally, endoreduplication is a rare phenomenon that results from failure in chromosome segregation leading to aberrant mitosis without proper anaphase, and the subsequent re-replication of non-split chromosomes that finally show up as diplochromosomes made up of four chromatids in the next mitosis (third S-phase). Using DNA staining to study the cell cycle, we didn't detect such cellular specie [3]. Besides, the observation that analogue incorporation for only one S-period, i.e. only in nascent DNA, does not result in endoreduplication, contrasting with endoreduplication when incorporation takes place for two consecutive rounds of replication, seems to point to the importance of template DNA for chromosome segregation. And, since in ACD-NRCC the template-DNA strand does not incorporate halogenated-nucleotides it is less likely that endoreduplication accounts to ACD-NRCC.

The most significant aspect of cells undergoing ACD-NRCC is whether they function differently and furthermore do they relate to stem-like cells. Thus, we recently published a work investigating the function of cells undergoing ACD-NRCC. We demonstrated that ACD-NRCC is not a result of quiescence; cells undergoing ACD-NRCC are actively dividing, and having similar viability, proliferation and cell cycle phase composition as controls. Moreover, we demonstrated ACD-NRCC in real time, in live cells. We showed that cells undergoing ACD-NRCC have a gene expression profile consistent with stem-cells gene expression profile. Finally, we demonstrated that cells undergoing ACD-NRCC are exquisite tumor initiating cells. They

initiated tumors with as little as 10 cells. And, thus one might be tempted to categorize these cells as stem-like cells [3, 4].

In conclusion, although, other investigators described variable effects generated by halogenated-nucleotides on cell proliferation and DNA replication, others and we could not confirm these findings. Thus, considering the tumor initiating capacity, stem-like gene expression profile exhibited by cells undergoing ACD-NRCC [3], and by the additional new data of large number of cells undergoing ACD-NRCC presented here, we could not conclude that our findings are due to an artifact.

Cell synchronization

To determine the degree of cell synchronization, we measured the actual cell cycle and each of its phases. We reasoned that in order to increase the potential number of cells undergoing ACD-NRCC that we can detect by the methods we used, it will be reasonable to have as many cells in the G0/G1 phase at the start point of the experiment. We would like to emphasize that synchronization was done to have as many cells as possible at the G0/G1 phase, and not because of any intrinsic need of cells undergoing ACD-NRCC. The more cells we can have at the start of the experiment ready to move into S phase (cells in G0/G1 phase) the more likely we are to detect ACD-NRCC that was presumed to be rare event in research reported by others, if ACD-NRCC occurs. To achieve that we carefully measured the duration of each cell line's cell cycle duration with its components (G0/G1, S and G2/M phases) over multiple experiments. We achieved on average about 55% synchronization i.e. 55% of the cells were in G0/G1 phase. To achieve that we performed optimization experiments using Aphidicolin and/or serum free media (SFM). The degree of synchronization at G0/G1 phase achieved with SFM was similar to the one

achieved with Aphidicolin; we chose to use SFM alone. The optimization experiments that helped us establish this methodology are described in Hari et al [4].

Image acquisition

The observers who acquired images, processed the images, scored them (asymmetric vs. symmetric), and determined what DNA content belonged to each nucleus were all blinded to cells identity. The scientists who labeled/stained cells, acquired images, processed image, and scored the images are all different persons. Additionally, one of us (IA) performed blinded validation of data to achieve a third tier of verification.

The association between cells undergoing ACD-NRCC and cancer-stem-cells

Based on this work, we can't attribute ACD-NRCC to cancer stem cells. However, recently we published a paper titled '*Tumor-initiating label retaining cancer cells in human gastrointestinal cancers undergo asymmetric cell division' [3]*; in that work, we describe how some cancer cells undergoing ACD-NRCC exhibit exquisite tumor initiating capacity and multipotency gene expression profile. Moreover, there are significant differences between cells undergoing ACD-NRCC and cells undergoing symmetric cell division in terms of stem-cells and pluripotency gene expression profiles. The former exhibit stem cells and pluripotency gene expression profile with certain genes like Sox2 being several hundred fold higher. In general, we hold the opinion that stem-like-cancer cell is a more appropriate term. Since we can't associate cancer stem cells or stem-like-cancer cells with ACD-NRCC based purely on the current paper and our previous work was just recently published and was not yet validated by an independent group, we used "putative stem-like-cells" in the body of the text. Interestingly, we are reporting in parallel that

cells undergoing ACD-NRCC (LRCC) in liver cancer and pancreatic cancer are extremely resistant to sorafenib and gemzar, respectively (data is not shown, and manuscripts are in preparation). These findings are consistent with the cancer stem cells hypothesis.

Cell fusion

This is an important issue that we attempted to deal with extensively using couple of lines of evidence. We showed a table to the Supporting Information (table S3) showing that without cytochalasin D the rate of couplets detection is 2.9% ± 1.7%, and with cytochalasin D the rate is over 50% (59.9% ± 1.0%). Couplets indicate two nuclei within the same cytoplasmic space without intervening cell membrane (as exhibited by the 3D rendering), and not simply two cells attached to each other. When we counted ACD, we counted number of ACD among all couplets, not as a percentage from all cells in the field, i.e. a percentage of cells arrested at mitosis. We discovered that without cytochalasin-D, we can't detect couplets that undergo ACD-NRCC, suggesting that our observations are less likely to be a result of cell-cell fusion. We set up the experiment, in terms of timing the arrest, to clearly detect two nuclei at telophase just before cytokinesis [3, 4]. Thus, we showed pictures of cells containing two nuclei not as yet separated sharing nuclear material and exhibiting ACD (figure 2, 6C, and S2). Furthermore, using similar methods, we demonstrated live cells undergoing ACD, in real time using confocal-cinematography [3]. In a different study, using some of the cells used in this study, we used genetic markers (HLA markers and in a separate experiment reporter genes introduced by a retroviral vector) to test for spontaneous fusion. We did not detect spontaneous fusion under these conditions [data is not shown as it belongs to a different experiment but we will be more than happy to share it]. Additionally, cells were plated singly and followed closely. During the

48 hours of the experiment no clusters formed, no collections of more than two cells mitigating extensive cell migration in 48 hours to fuse to other cells. Another line of evidence mitigating cell fusion is the functionality of these cells. We showed evidence that we do not detect ACD if we block Wnt. Unless Wnt is also involved with cell-cell fusion (as such no reported evidence) it further suggests that our observations are not due to fusion. Using the double labeling technique on live cells, we demonstrate that when we isolate cells labeled with both-nucleotides just before the second mitosis, and after the completion of the second mitosis these cells generate two species of cells: Cells containing both nucleotides and cells containing only one nucleotide suggesting ACD. Cells containing both nucleotides, upon division will generate two daughter cells containing both nucleotides but here we show that these cells also generate cells containing one of the nucleotides (second) demonstrating ACD. We showed a new dot-plot diagram demonstrating this observation (figure S3). Finally, cells undergoing ACD are functionally different from other cancer cells unlikely to be due to fusion i.e. if two cancer cells simply fuse why would they exhibit as a result completely different phenotype such as stem-like cancer cells; in Xin et al. we show that cells undergoing ACD-NRCC are exquisite tumor initiating cells with stem-cells and pluripotency gene expression profile [3].

The potential effect of Karyotype on ACD-NRCC

We elected to do Karyotyping on the 2 colorectal cell lines derived from surgical specimens. The results are presented in Supporting Information figure S9. The important question regarding the karyotype: If ACD-NRCC exist how are various karyotypes affects it? We did not detect significant differences in the rate of ACD-NRCC between the various karyotypes. We also did not detect difference in terms of isolated cells undergoing ACD-NRCC ability to initiate tumors.

However, these question deserve a separate paper and in depth examining of the effects of various karyotyping on ACD-NRCC. We feel that the full gamut of the answer to this question is beyond the scope of this work. However, we hypothesize that using the methods used in this work even if part of the chromosomal complex undergoes ACD-NRCC due to potential different karyotypes it will still be detected by these methods. The question is what are the functional consequences of such cells? A question we plan to follow-up in a separate study.

The potential role of Wnt pathway in cells undergoing ACD-NRCC

We performed experiments to further test the potential role of Wnt in ACD-NRCC. We performed experiments using the Wnt antagonist IWP-2 (figure 6 and S8). We found that IWP2 reduced the expression level of TCF4 by 64%, and decreased the amount of cells undergoing ACD-NRCC between 5-to-10 folds (measured by flow-cytometry). The effect of Wnt antagonist on TCF4 was noticed both on gene expression and protein expression levels. Using the in-situ fluorescence double labeling assay, IWP2 and siRNA-TCF4 abolished completely our ability to detect cells undergoing ACD-NRCC (figure 6C-D). Additionally, after treatment with IWP2, we could not detect asymmetric distribution of TCF4 protein. To validate these results, we used qRT-PCR (figure 6E). We found that IWP2 reversed or reduced the expression of TCF4, TCF7, Sox17 and CSNK2A1 (figure S5 and 6E). Previously these 4 genes were differentially expressed, upregulated in ACD-NRCC vs. symmetrically dividing cells. These results implicate the Wnt pathway, and TCF4 in ACD-NRCC, and argue against the fusion hypothesis.

Cells undergoing ACD-NRCC do not necessarily indicate also ACD by fate

We would like to mention that the reason we associated in this paper ACD-NRCC with stem-like-cancer cells is based on our previous work published recently [3]. In that work, we demonstrated that cells undergoing ACD-NRCC have an exquisite ability to initiate tumors when compared to cells not-undergoing ACD-NRCC. Cells undergoing ACD-NRCC initiated tumors with 10 cells. And, the tumors generated both ACD-NRCC cells (minority) and cells not-undergoing ACD-NRCC (majority) suggesting at least bi-potency. We showed that cells undergoing ACD-NRCC have gene expression consistent with pluripotency/stem-cells gene expression profile. Additionally, we showed ACD-NRCC in real time and in live cells using confocal cinematography. Thus, we are more confident that our observation of ACD-NRCC is a real phenomenon. However, our current data don't reveal whether the observed ACD-NRCC is also ACD that lead to different cell fate. Our line of reasoning was based on the fact that in the paper we recently published we felt we had enough evidence to associate ACD-NRCC to tumor initiating cells with stem-like gene expression profile. Since this paper was just recently published and was not validated as yet by independent investigators, we will avoid associating between ACD-NRCC and cancer-stem-cells.

ACD-NRCC rate is low: Possible interpretation

The ACD-NRCC frequency seems low, ranging from 1-to-6%, but this could be the nature of this phenomenon. This is one of the problems in the field making this hypothesis controversial. Except one example showing nearly 50% ACD-NRCC during muscle progenitor cell division in vivo [9], all other reports showed ACD-NRCC in only a few percent of cells if any. The observations of low rate of ACD-NRCC by others and us could indicate spurious observations but the functional findings presented in Xin et al. [3] mitigate this argument.

Permit us to introduce another possible interpretation of these observations. Based on the fact that only one report in the literature reported on more than a single digit percent of cells undergoing ACD-NRCC, and our own data encompassing literally over a hundred separate experiments (past and present on-going experiments in our lab) we offer the following interpretation: It is possible that the rate of cells undergoing ACD-NRCC is somewhat constant, for a given condition, and in the few percent range. If ACD-NRCC is a trait of stem-like cells [3], and if ACD-NRCC suggest one of several modes of self-renewal than it is possible that only a few percent of cells should undergo ACD-NRCC at any given time point. Thus, if cells undergoing ACD-NRCC are preferentially located to the SP fraction, and at steady state one detects 1.5% ACD-NRCC in the whole cell population that does not necessarily indicates that if we test for ACD-NRCC in isolated SP cells we will get much higher rate of ACD-NRCC. Our interpretation of these results point to the fact that it is possible that at such conditions, with fewer cells in the culture dish, SP cells divide symmetrically to increase and replenish the volume of cells, possibly until more contact inhibition is detected by the cells or until a certain balance/steady state is achieved (reminiscent of fast repair of an injury). At the time point where more cells are in the culture, more confluency, with more and more contact inhibition, the SP cells achieve a certain balance, steady state and some SP cells start to function as self renewing cells and undergo more ACD-NRCC. We also hypothesize that ACD-NRCC must be somewhat constant at a given state of conditions based on our observations. Clearly, these hypotheses need further investigation possibly another project that needs to be explored in our group. Finally, once one isolates SP cells and cultures them they begin to generate non-SP cells immediately in

culture (reported previously by other investigators), thus after 24 hours one can not get a pure population of SP cells. At best, it is a population of cells enriched for SP cells [10].

Supplementary Methods

Nota bene: All human surgical specimens were obtained and processed under NCI protocol 09-C-0079 approved by the NCI-IRB and after obtaining proper consent from the patients. All animal experiments were approved by the NCI-IRB for animal experimentation.

Cells

All cells used in this study are listed in the table S1 with information of their source and culturing conditions.

Establishment of short human cancer cell lines from fresh tumors

In order to obtain fresh tumors, after obtaining consent, patients were enrolled on our tissue procurement protocol, approved by the NCI/NIH IRB. Tumors were harvested from patients (IRB Protocol: 09-C-0079). Tumors were brought to the laboratory from the operation room immediately after resection and worked aseptically. Tumors were washed briefly with cold 1X HBSS, minced into 1-3 mm chunks and transferred into gentleMACS C tubes (Miltenyi Biotec) containing dissociation medium. Dissociation medium contained DMEM/F12 (1:1) growth medium supplemented with collagenase, type IV (1g/L) and pulmozyme (DNase, Dornase alfa inhalation solution) 10,000U/L. Minced tumors were dissociated gently by the programmable gentleMACS Dissociator (Miltenyi Biotec) to yield cell suspensions with a high viability rate.

Cell suspension was filtered through sterile 70 µm filter and washed with 1XHBSS. Cells were resuspended with appropriate growth medium and plated into ultra low attachment tissue culture flasks at a concentration of 1 million/ml for spheroid formation. Spheroids were collected after 6 days and either cryopreserved. Spheroids then were transplanted into nude mice (*nu-/nu-*). Xenografts were harvested, re-dissociated, and used in this experiment. Single cell suspensions from these xenografts were maintained and cultured for further experiments [11]. Short-term cultures of human melanoma fresh tumors were obtained as described before [12, 13].

Growth curves and doubling times

In order to maximize the quantitative and qualitative detection rate of asymmetrically dividing cells, we had to synchronize the cell cycle according to each cell line's and the fresh tumors doubling times. In 15 to 18 wells of 6-well plates, 5×10^4 cells were plated per well and allowed to attach for 24 hours. On each time point, 8 hours apart, the numbers of live cells were determined in three wells. Acquired numbers were averaged and converted into percentage relative to the average acquired at the first time point. These percentages were plotted using Excel spreadsheet. A best fit exponential trend line with y-axis interception at 100% was generated and by using regression analysis of this trend line the doubling time was computed (table S2). Correlation value $R^2 \geq 0.9$ was considered adequate for computations of doubling times. Doubling times were calculated for all cells tested.

DNA double-labeling-procedure

DNA double labeling was performed with modifications, as previously described by Rando et al. (figure 1B and figure S1A) [9]. Iodo-deoxyuridine (IdU) and chloro-deoxyuridine (CldU) were

purchased from Sigma (USA) and used at a final concentration of 5 uM. Extensive experiments for optimization of nucleotide incorporation efficiency were performed. According to the cell doubling times determined above (table S2), cells were first synchronized in serum-free media (SFM) for one cell doubling time. This was done in order to obtain as many cells as possible at the G1/G0 phase before the initiation of the double labeling experiment (figure 1B and figure S1A). For the first DNA replication cycle, cells were labeled with the first thymidine analog either IdU or CldU in complete growth media. Before the start of the second DNA replication cycle, growth media were replaced with SFM again. At the completion of the first cell cycle, cells were trypsinized and plated singly in collagen IV-coated 8-well chamber slides (Ibidi, Germany) in complete growth media containing the second thymidine analog either CldU or IdU. Before the completion of the second cell cycle, growth media were replaced with SFM containing Cytochalasin D (2 μM final concentration; Sigma) to arrest cells at cytokinesis. Arresting cells at cytokinesis afforded us observing cells (couplets) at division while avoiding the confusion with fused cells or two cells attached to each other. Extensive control experiments were performed with and without Cytochalasin D demonstrating that the observed asymmetric divisions were not spurious observation due to cell fusion or because cells were attached to each other (one of the reasons that cells were plated singly). Subsequently, cells were then fixed for immunofluorescence staining. The specificity and sensitivity of IdU and CldU labeling and the effects of cytokinesis arrest by Cytochalasin D are shown in figure S1B. We used a Wnt3-agonist because it is expressed both in cells undergoing ACD-NRCC and cells undergoing SCD. 10 uM of IWP2 (Stemgent) were added to the SFM or growth media in the IWP2 treatment conditions. siRNA-TCF4 (ON-TARGETplus, Dharmacon) or control siRNA (Dharmacon) was transfected into cells during the first SFM synchronization step using Lipofectamine-2000 according to

manufacturer instruction (Invitrogen). A final concentration of 33nM of either siRNA-TCF4 or control siRNA were used.

Immunofluorescence staining

Immunofluorescence staining was performed as previously described by Randon TA et al. with modifications . Mouse monoclonal antibodies, clone B44, recognizing IdU, conjugated with FITC, was obtained from BD Biosciences (San Diego, California, United States) and used at a dilution of 1:10~1:20. Rat antibody clone BU1/75 (ICR1) recognizing CldU was purchased from Novus Biologicals (Littleton, Colorado, United States) and used at a dilution of 1:500. This antibody was detected using an anti-rat secondary antibody, Alexa 546-coupled (Invitrogen/Molecular Probes, Carlsbad, California, United States), and used at 1:2,000. For detection of labeled DNA, cells were fixed in 70% ethanol overnight at 4C, denatured in 2.5 M HCl for 30 min, permeabilized in 0.25% Triton-X-100 for 5 min, and blocked in PBST (PBS with 0.1% Tween-20) supplemented with 10% FBS for one hour at RT before incubation with primary antibodies in PBST with 10% FBS overnight at 4C. The secondary antibody was incubated for one hour at RT. Subsequently, slides were dried and mounted with Vectashield (Vector Laboratories, Burlingame, CA, USA) or Slow-Fade Gold (Invitrogen/Molecular Probes, Carlsbad, California, United States) containing DAPI. Specificity of the anti-CldU and anti-IdU primary antibodies and the secondary antibody were tested extensively (figure S1B).

Fluorescence confocal microscopy

In order to detect couplets of cells arrested in cytokinesis, we scored only couplets that were well isolated from other cells. Clusters of more than two cells were rare and never investigated for

asymmetric division as to avoid spurious results due to cell aggregation. Importantly, the observers who acquired images, processed the images, scored the images (asymmetric vs. symmetric), and determined what DNA content belonged to each nucleus were all blinded to the cells identity. The scientists who labeled/stained cells, acquired images, processed image, and scored the images are all different persons. Additionally, one of us (IA) performed blinded validation of data to achieve a third tier of verification. Nota bene, for the second cell cycle, cells were plated singly to enhance efficiency of couplets identification. Approximately 100-130 couplets were scored per condition, and all experiments were done in triplicates (n=3 to 15). Confocal images were sequentially acquired with Zeiss AIM software using a Zeiss LSM 510 NLO Confocal system (Carl Zeiss Inc, Thornwood, NY) with a Zeiss Axiovert 200M inverted microscope and 2-photon laser tuned to 760 nm, a 25 mW Argon visible laser tuned to 488 nm, a 1 mW HeNe laser tuned to 543 nm and a 5 mW HeNe laser tuned to 633 nm. Either a 40x Plan-Neofluar 1.3 NA or a 63x Plan-Apochromat 1.4 NA oil immersion objective was used at zoom settings from 2 to 5. Emission signals after sequential excitation of DAPI, Alexa Fluor 488 and Alexa Fluor 568 by the 760 nm, 488 nm or 543 nm laser lines were collected with a BP 390-465 filter, BP 510/20 filter or BP 565-615 filter, respectively, using individual photomultipliers. TCF4 intensity was measured using LSM ImageBrowser 4.0 (Zeiss). Z-stacks consisted of 30 to 50 slices at 0.38μm intervals and these stacks were used with Bitplane's (Zurich, Switzerland) Imaris software (v6.0) for surface rendering. To clearly define the positions of two nuclei in the same cytoplasmic space, a cutting plane was used to expose internal surfaces or outer surfaces were made semi-transparent.

Detection and isolation of live cells undergoing ACD-NRCC

Live cells undergoing ACD-NRCC were isolated using double-labeling and double-sorting as described below (figure S3) [3, 4]. Human gastrointestinal cancer cells grown in flasks were first arrested at G0/G1 phase with serum-free media for one cell cycle, plated at 5e6 cells per T175 flask in growth media without antibiotics, microporated before S phase as above with unlabeled dUTP (100μM) as a control or with the labeled-nucleotide Cy5-dUTP (100μM), and cultured to allow completion of the first labeling cell cycle. Then cells were microporated before S phase again with Alexa555-dUTP (100μM, Invitrogen) or unlabeled-dUTP, respectively, and sorted by FLOW CYTPMETRY for Alexa555+ high /Cy5+ high cells before the completion of the second labeling cell cycle. The double positive cells (Alexa555+ high/Cy5+ high) were re-run to make sure they were pure, cultured to allow the completion of their second labeling cell cycle and sorted for the Alexa555+/Cy5- cells (cells undergoing ACD-NRCC) and Alexa555+/Cy5+ cells (cells undergoing symmetric cell division). CFSE staining (5.0 uM for 15 min, Invitrogen) was used to monitor the cell cycle. 10 uM of IWP2 (Stemgent) was added to the SFM or growth media in the IWP2 treatment conditions.

Detection and isolation of live label retaining cells (LRC)

Detection and isolation of live label retaining cells (LRC) were performed as described before and here in supporting protocol [3, 4]. Live LRC and non-LRC were isolated as follows from various cell lines, established fresh primary gastrointestinal tumor cells as well as benign liver cells. Human cancer cells grown in flasks were first arrested at G0/G1 phase with serum-free media for one cell cycle, re-plated at 5e6 cells/T175 flask in growth media without antibiotics, then labeled with dUTP (100 uM) as a control or with the Cy5-dUTP (100 uM) from VWR before S phase by microporation (Invitrogen). Microporation was done according to the

manufacturer's instruction. Briefly, 60e6 cells cultured in antibiotics-free growth media were trypsinized, harvested and washed with PBS once. 5e6 cells were resuspended in 108 ul of R-buffer purchased from Harvard Apparatus and mixed with 12 ul of either dUTP or Cy5-dUTP (100 uM). Cells were loaded into 100 ul tip and into the microporation tube containing 3 ml of microporation buffer, and microporated at 1400 V for 20 millisecond twice, then transferred immediately to growth media without antibiotics for culture at 37°C. After one complete cell cycle Cy5+ cells were sorted by FLOW CYTPMETRY (BDFacsAriaII, BD Biosciences, San Jose´, CA). A population of Cy5+ cells comprising approximately 60% of the total viable cells was sorted and re-ran to make sure Cy5+ high cells were more than 99% pure. The Cy5+ high subpopulation was propagated in log phase in culture for eight cell cycles. Then Cy5+ cells were gated based on the unlabeled dUTP-microporated cells and sorted as LRC, and 8-10% of total viable cells with lowest Cy5 were sorted as Cy5- cells or non-LRC for subsequent analysis.

Cell viability and toxicity assays

Cell viability was measured using the cell counting kit-8 (Dojjindo, Japan) according to the manufacturer protocol. 3000 cells were plated in each well of 96-well plates. Cells were microporated with either dUTP control, Cy5-dUTP or Alexa555-dUTP. 10 uM of IWP2 (Stemgent) were added to the SFM or growth media in the IWP2 treatment conditions. Cell viability was measured as absorbance at 450 nm. Cell toxicity was measured using the ApoTox-Glo assay kit (Promega, Madison, WI) according to the manufacturer protocol. Cells were plated in each well of 96-well plates. Cells were microporated with either dUTP control or Cy5-dUTP.

Cell toxicity was measured as luminescence using filters of Ex490/Em510-570. Please also see supporting protocol.

Cell karyotyping

The cells were treated with colcemid (Karyomax, Invitrogen) (10ug/ml) for 2 hours prior to harvest. Cells were dissociated with Trypsin/EDTA (0.05%), treated with hypotonic solution (KCL 0.075M) for 15 minutes at 37°C and fixed with methanol: acetic acid 3:1. G banding patterns were obtained with trypsin treatment followed by Giemsa stain [14]. Analyses were performed under an Axioplan 2 (Zeiss) microscope coupled with a CCD camera; images were captured with Band View 6.0 karyotyping software, (Applied Spectral Imaging Inc., Vista, CA). A minimum of 10 mitoses was examined per cell line.

Isolation and analysis of the side population

To isolate the side population, cells at near confluence were first trypsinized, mixed with growth media, spun down at 1000 rpm for 4 min and resuspended in growth media at 1e6 cells/ml. Cells were then transferred to 125 ml culture flasks (10-30 ml/flask, Triforest Labwares) with or without 100 uM Verapamil (Sigma) in the dark, kept in a 37C incubator for 20 minutes. Hoechst33342 (Invitrogen) was then added to a final concentration of 10 ug/ml in dark and cells were kept in a 37C incubator for 90 minutes with shaking every 20 minutes. Cells were then kept on ice for 5 min, and subsequently kept in dark and on ice in all following steps. 7-aminoactinomycin D (7-AAD, Invitrogen) was added to a final concentration of 2 ul/ml, and cells were incubated on ice for 20 min. Cells were filtered through 40 um cell strainers (BD Falcon), spun down, and resuspended at 1.5e7 cells/ml in cold FLOW CYTPMETRY collection

media (49.5% growth media, 49.5% FBS plus 1% of 1M Hepes buffer) for sorting by FLOW CYTPMETRY (The Vantage SE sorter, BD, USA). 7-AAD positive cells were gated first. The side population was then identified after gating the Verapamil or Fumitrimorgin treated control cells (figure S4). The non-side population was identified as high Hoechst33342 eells. Both side population and non-side population were sorted separately, washed with serum-free media, plated in growth media and cultured for one week, two weeks or five weeks before testing for asymmetric cell division.

CD133+ cell isolation

CD133+ and CD133- cells were isolated by MACS using the indirect CD133 MicroBead kit (Miltenyi Biotec Inc., Auburn, CA, USA) according to manufacturer's manual. MACS magnetic separator, MS columns, 30 μm nylon mesh pre-separation filters, autoMACS running buffer were purchased from Miltenyi Biotec Inc. Briefly, cells at near complete confluence were trypsinized, mixed with growth media, spun down, resuspended in autoMACS running buffer and passed through the pre-separation filters. Cells were spun down and resuspended in the autoMACS running buffer, mixed with FcR blocking reagent, CD133/1 (AC133)-biotin and incubated at 4C for 10 minutes. Then cells were washed twice with 10 ml of MACS buffer, resuspended in MACS buffer, mixed with anti-biotin MicroBead, and incubated for 15 minutes at 4C. After washings, cells were loaded onto pre-rinsed MS columns and unlabeled CD133- cells were collected. Next, the MS column was washed and removed from the magnetic separator and the labeled CD133+ cells were collected. To increase the purity, the cells were enriched over a second column for a second CD133+ or CD133- cells MACS sorting. Sorted cells were plated at a concentration of 5e4 cells per well of six well plates in complete growth media and

incubated for just over 9 days. Then, cells were labeled for analysis of ACD-NRCC as described above.

Dual chamber assay

5e4 sorted CD133+ or CD133- cells were cultured in each well of 6-well plates containing inserts that has 0.22 μm diameter semi-permeable membranes. 1e5 CD133- or CD133+ cells were plates in the insert. The cells were cultured for just over 9 days, then, cells in the lower chamber were labeled for analysis of ACD-NRCC as described above.

Conditioned media

Conditioned media were collected from single wells or dual chambers under specific conditions, aseptically filtered through 0.22 μm filter units, and mixed with normal growth media. CD133+ cells were cultured in conditioned media for one week in a 1:4 ratio (one part conditioned media-to-four parts fresh media), and the conditioned media was replaced every 24 hours (figure 4A). CD133+ or CD133- cells were exposed to the various filtered and pre-mixed conditioned media as shown in figure 4A . To test whether the conditioned media contained a potential factor capable of inducing asymmetric cell division, the conditioned media from CD133-/CD133+ dual chamber was boiled for 5 minutes and used as above, 5% FBS was added to the conditioned media to a total protein concentration equal to normal growth media (figure 4. pH, specific gravity and protein concentrations of the conditioned media were determined with Checker pH Meter (HANANA instruments, USA), Specific Gravity Bottle (Crystalgen, Inc., USA) and NanoDrop ND-1000 Spectrophotometer (Thermo Fisher Scientific, USA), respectively. There were no differences in these parameters between the regular growth media and the heat

denatured media. The p values are in comparison to positive control i.e. CD133-positive cells grown in conditioned media from dual chambers, figure 4A).

Wnt pathway protein asymmetric distribution assay

To detect asymmetric distribution of Wnt pathway proteins, we used the same method as described earlier for the detection of ACD-NRCC by DNA double labeling and cytokinesis arrest (figure 1B and figure S1A). Instead of labeling and detection of DNA, we detected protein asymmetric distribution between daughter cells in cytokinesis-arrested cell couplets by immunocytochemistry as follows. The cells were washed with PBS, fixed with 4% paraformaldehyde for 15 minutes at room temperature, washed 3 times with PBS (5 min each wash), permeablized with 0.25% triton-x-100 for 5 min at room temperature and washed 3 times with PBS as above. Antigen retrieval was applied for detecting APC by heating at 120°C in 10ml of sodium citrate buffer (10 mM sodium citrate, 0.05% tween 20, pH 6.0) in a pressure boiler. After washing with PBST, cells were blocked with PBST plus 1% BSA at 37ºC for 45 minutes. The six rabbit primary antibodies from Abcam were diluted in PBST plus 1% BSA at the given concentrations (Frizzled, 1:10; LRP5, 1:10; Axin2, 1:100; APC, 1:50; β-catenin, 1:200; TCF4, 1:200) and incubated with the cells at RT for 2 hours. After washing, the cells were incubated with the secondary antibody (Alexa-488 donkey anti-rabbit, 1:200, Invitrogen) in PBST plus 1% BSA for 1 hour, washed 3 times as above and air-dry in dark. Then approximately 100µl of Slow Fade Gold (Invitrogen) was added to each well for confocal microscopy examination. Couplets were identified and photograph.

Gene expression analysis

We FLOW CYTPMETRY sorted various human gastrointestinal cancer cells undergoing ACD-NRCC and control cells undergoing symmetric cell division as described above. Cells were lysed, and total RNA was isolated and treated with DNase using miRNeasy Mini kit and RNase-Free DNase Set (QIAGEN) following the manufacturer's protocol. Total RNA was quantified using spectrophotometry (Nanodrop, Wilmington, DE). All reagents for genomic DNA elimination, reverse-transcription, pre-amplification and real-time qPCR array were purchased from SABiosciences (Frederick, MD) and all real-time qRT-PCR experiments for Human Stem Cell Pathway Array, Human Wnt Pathway Array were done in triplicates following the manufacturer's protocol. For genomic DNA elimination, 2 µl of 5X genomic DNA elimination buffer was added to 8µl of RNA and the mixture was incubated at 42ºC for 5 minutes and immediately chilled in ice. The RT cocktail was then made with the following materials: 4 µl of BC3 (5X reverse transcription buffer 3), 1 µl of P2 (primer and external control mix), 1 µl of RE (cDNA Enzyme Synthesis Mix), 1 µl RI (RNase Inhibitor), and 3 µl of RNase free water for a total volume of 10 µl. 10 µl of the RNA from which genomic DNA had been eliminated was added to the 10 µl of the RT cocktail and incubated at 42ºC for 30 minutes. The reaction was stopped by heating at 95ºC for 5 minutes. For pre-amplification of cDNA target templates, the Nano PreAmp PCR cocktail mix was prepared by mixing 12.5 µl of the RT^2 PreAmp PCR master mix and 7.5 µl of the RT^2 Nano PreAMP cDNA synthesis Primer Mix for human stem cell pathway array, human Wnt pathway array and customized array. 5 µl of the first strand cDNA synthesis reaction mix were added to the 20 µl of the nano PreAmp PCR cocktail mix, pre-amplified at the following condition: 95ºC for 10 minutes followed by 12 cycles of 95ºC 15 seconds and 60ºC 2 minutes. After PCR, the tubes were put on ice. 2 µl of the side reaction reducer (SR1) was then added to each pre-amplified reaction, incubated at 37ºC for 15 minutes

followed by heat inactivation at 95ºC for 5 minutes. 84 µl of Rnase-DNase free water was then added to each 27 µl of nana PreAMP PCR reation. Real-Time qPCR was accomplished using the SABioscience RT^2 master mix and a 384 well plate for human stem cell pathway array, human Wnt pathway array and customized array using ABI 7900 HT system (Applied Biosystems, Foster City, CA) following the supplier's protocol. 1665 µl of the 2x SABioscience RT^2 qPCR master Mix, 50 µl of the diluted first strand cDNA synthesis reaction and water were mixed in the total volume to 2700 µl. 10 µl of the above mixture was then added into each well of a 384 well PCR array plate. The plate was then placed in the real time thermal cycler for real time qPCR amplification at the following condition: 95ºC for 10 minutes followed by 40 cycles of 95ºC 15 seconds and 60ºC 2 minutes. Ct values were analyzed using the company's online software. Primers for the individual genes of TCF4, TCF7, SOX17 and CSNK2A1 were designed by and purchased from Qiagen, and real-time qRT-PCR was performed using the same conditions as above. Gene pathway analysis was done using Ingenuity Pathway Analysis online software (IPA 9.0).

Statistics

(A) The first objective was to determine the statistical significance of observing asymmetric cell division via non-random chromosomal cosegregation ACD-NRCC. The theoretical probability of detecting a single cell that underwent asymmetric cell division via non-random chromosomal cosegregation would be extremely small (one-in-2^{23} cell divisions), <0.00001 for any given experiment. For any given experiment in which one or more asymmetric cell divisions via non-random chromosomal cosegregation are identified, the two-tailed p-value for the exact binomial test of whether the observed fraction is equal to any value of 0.00001 or less is <0.0001. Thus,

any instances in which at least a single asymmetric cell division via non-random chromosomal cosegregation would be identified would be extremely unlikely to occur by chance. For the combined experiments, detecting non-random asymmetrically dividing CD133+ cells that were cultured in conditioned media from dual chamber experiments, with 14/512 having non-random asymmetric cell divisions, by an exact binomial test against a null hypothesis of 0.00001 as a potential fraction, the p-value is <0.0001. (B) The second objective was to determine if the data with respect to the observed effect of the niche on asymmetric cell division via non-random chromosomal cosegregation by the putative stem-like cancer cells (figure 4A) is statistically significant. CD133+ or CD133- cells cultured alone did not exhibit ACD-NRCC. However, CD133+ cells cultured with 20% conditioned media from dual chamber cultures exhibited ACD-NRCC. The results of the experiments conducted for a given condition were all sufficiently homogeneous to be combined together to form an overall fraction; in fact the condition with the greatest variation (CD133+ dual chamber), had a p-value of 0.75 for a two-tailed test of homogeneity of fractions using Mehta's modification to Fisher's exact test. Thus, the following fractions of cells were compared overall using Mehta's modification to Fisher's exact test: The resulting p-value for this overall comparison was: p=0.019. Thus, there is some evidence that at least one of the pairs of fractions differs from another. Selecting the two most important fractions to evaluate the niche effect on ACD-NRCC and the two most extreme fractions, 14/512 (CD133+ cells exposed to dual chamber conditioned media) vs. 0/511 (CD133+ cultured in conditioned media from CD133+), the p-value for that comparison is 0.0001, by Fisher's exact test. Other extreme comparisons were: 14/512 (CD133+ cells exposed to dual chamber conditioned media) vs. 0/200 (CD133- cultured alone in normal media) has a p-value of 0.014, by Fisher's exact test, and 14/512 (CD133+ cells exposed to dual chamber conditioned media)

vs. 0/202 (CD133+ cultured alone) has a p-value of 0.014. Thus, CD133+ exposed to conditioned media from a dual chamber would tend to differ from CD133+ exposed to conditioned media from CD133+ alone, CD133+ alone in normal media and CD133- cultured alone in normal media. (C) To test for significance of the relative proportions of cells undergoing ACD-NRCC between tested groups, we used the Poisson method (figure 3C and the other SP experiment).

References:

1. Pera MF, Tam PP. Extrinsic regulation of pluripotent stem cells. Nature. 2010; 465: 713-20.
2. Park IH, Zhao R, West JA, Yabuuchi A, Huo H, Ince TA, et al. Reprogramming of human somatic cells to pluripotency with defined factors. Nature. 2008; 451: 141-6.
3. Xin HW, Hari DM, Mullinax JE, Ambe CM, Koizumi T, Ray S, et al. Tumor-initiating label-retaining cancer cells in human gastrointestinal cancers undergo asymmetric cell division. Stem Cells. 2012; 30: 591-8.
4. Hari D, Xin HW, Jaiswal K, Wiegand G, Kim BK, Ambe C, et al. Isolation of live label-retaining cells and cells undergoing asymmetric cell division via nonrandom chromosomal cosegregation from human cancers. Stem Cells Dev. 2011; 20: 1649-58.
5. Marks J. Long shadow of Linnaeus's human taxonomy. Nature. 2007; 447: 28.
6. Leuner B, Glasper ER, Gould E. Thymidine analog methods for studies of adult neurogenesis are not equally sensitive. The Journal of comparative neurology. 2009; 517: 123-33.
7. Cortes F, Pastor N, Mateos S, Dominguez I. The nature of DNA plays a role in chromosome segregation: endoreduplication in halogen-substituted chromosomes. DNA repair. 2003; 2: 719-26.
8. Cantero G, Mateos S, Pastor N, Cortes F. Halogen substitution of DNA protects from poisoning of topoisomerase II that results in DNA double-strand breaks. DNA repair. 2006; 5: 667-74.
9. Conboy MJ, Karasov AO, Rando TA. High incidence of non-random template strand segregation and asymmetric fate determination in dividing stem cells and their progeny. PLoS biology. 2007; 5: e102. doi:06-PLBI-RA-2054R2 [pii]
10.1371/journal.pbio.0050102.
10. Haraguchi N, Utsunomiya T, Inoue H, Tanaka F, Mimori K, Barnard GF, et al. Characterization of a Side Population of Cancer Cells from Human Gastrointestinal System. Stem cells (Dayton, Ohio). 2006; 24: 506-13. doi:10.1634/stemcells.2005-0282.
11. Ray S, Langan RC, Mullinax JE, Koizumi T, Xin HW, Wiegand GW, et al. Establishment of human ultra-low passage colorectal cancer cell lines using spheroids from fresh surgical specimens suitable for in vitro and in vivo studies. Journal of Cancer. 2012; 3: 196-206.
12. Yannelli JR, Hyatt C, McConnell S, Hines K, Jacknin L, Parker L, et al. Growth of tumor-infiltrating lymphocytes from human solid cancers: summary of a 5-year experience. International journal of cancer. 1996; 65: 413-21.

13. Topalian SL, Solomon D, Rosenberg SA. Tumor-specific cytolysis by lymphocytes infiltrating human melanomas. J Immunol. 1989; 142: 3714-25.
14. Seabright M. A rapid banding technique for human chromosomes. Lancet. 1971; 2: 971-2.